High photosynthetic rates associated with pico and nanophytoplankton communities and high stratification index on the North West Atlantic Shelf.

Alex Robinson[1□], Heather Bouman[1], Gavin Tilstone[2*], Shubha Sathyendranath[2]

[1]*Department of Earth Sciences, University of Oxford, South Parks Road, Oxford, OX1 3AN, UK.*

[2]*Plymouth Marine Laboratory, Prospect Place, West Hoe, Plymouth, PL1 3DH, UK.*

[□]*Current address: Centre for Ecology and Hydrology, MacLean Building, Benson Lane, Wallingford, Oxon, OX10 8BB, UK.*

***Corresponding author:** Dr. Gavin Tilstone, ghti@pml.ac.uk

Running title: Phytoplankton succession and photosynthesis.

KEY WORDS: Atlantic Ocean, Phytoplankton size, Phytoplankton succession, Photosynthesis Parameters.

Abstract

The biological dynamics of pelagic marine ecosystems are strongly influenced by the size structure and ecological succession of phytoplankton, which in turn modifies photosynthetic efficiency. Variability in photosynthetic rates is closely coupled with changes in community structure, but it is difficult to obtain coincident data at high enough resolution to characterise these changes. In this study, we employ hierarchical cluster analysis on chlorophyll-normalised high performance liquid chromatography (HPLC) pigment concentrations from the North West Atlantic shelf, to identify seasonal successional trends amongst phytoplankton populations. Changes in phytoplankton community were also analysed as a function of mean equivalent spherical diameter (MESD) derived from absorption measurements, photosynthetic rates, water-column stratification and temperature. Well-mixed conditions in spring to early summer were associated with populations of large cells containing high concentrations of fucoxanthin, chlorophyll-*c*1 and chlorophyll-*c*2 relative to chlorophyll-*a* (Chl *a*). As stratification increased over the course of the summer, these cells were replaced by populations dominated by chlorophyll-*b*, 19'-hexanoyloxyfucoxanthin, 19'-butanoyloxyfucoxanthin and divinyl chlorophyll-*a,* indicative of small picophytoplankton. As stratification decreased in autumn, MESD and alloxanthin increased, suggesting the presence of cryptophytes. Positive relationships were found between MESD and the quantum yield of photosynthesis (φ_m) for 7 out of the 8 phytoplankton clusters identified, while negative relationships between mean mixed layer photosynthetically active radiation and φ_m and the light limited slope of photosynthesis (α^B) were observed for 4 clusters, as a result of nutrient limitation and photo-protection. The highest photosynthetic rates were associated with a pico & nanophytoplankton communities, which increased from spring to late summer as stratification intensified. By contrast, diatom communities had the lowest photosynthetic rates throughout the year. These successional patterns in the dominant phytoplankton size-

class and phenology support Margalef's mandala in terms of the relationship between turbulence and community structure. The study sheds new light on assemblages dominated by smaller cells, under warm, stratified conditions, having higher photosynthetic efficiencies, which has implications for the carbon flux on the NW Atlantic shelf.

1. Introduction

The ecological functioning of marine phytoplankton communities is strongly influenced by the species present and their size (Chisholm 1992, Raven 1998). There are more than 5000 species in the global ocean, which have a 1000 fold range in cell size (Jiang et al., 2005). In the North Atlantic, cell size varies from ~0.6 μm to >1000 μm, which is highly correlated with seasonal changes in water column stratification (Kiørboe 1993). Large phytoplankton, especially diatoms, thrive in turbulent and partially mixed waters that are rich in nitrate, which facilitates rapid assimilation of nutrients and carbon fixation (Pahlow et al., 1997). Smaller cells that comprise the picophytoplankton, tend to inhabit nutrient poor, stratified, oligotrophic regions which are highly stratified (Munk and Riley,1974; Malone, 1977). Margalef (1978) proposed a mandala to divide phytoplankton groups according to the levels of turbulence and nutrient availability.

Phytoplankton productivity in the North Atlantic accounts for ~50% of the global ocean production (Wassmann, 1990), which has huge implications for the ocean biological carbon pump (Daniels et al., 2015). The classic theory of succession in this region is that spring bloom forms as the winter mixed-layer shoals, exposing high nutrient concentrations in the surface layers to light as incident irradiance and day length increase (Sverdrup, 1957). The spring bloom is often dominated by diatoms, which are replaced by nanophytoplankton as nutrients become depleted (Margalef, 1978). Different hydrographic circulation patterns

can ~~cause~~ modulate the recycling and regeneration of nutrients in the euphotic zone which can lead to successional changes in pico, nano and microphytoplankton (e.g. Clarke et al. 2016). New methods of detection of phytoplankton functional types from satellite data similarly illustrate an annual succession between diatoms, nanophytoplankton and *Prochlorococcus* (Alvain et al. 2008). These successional changes modify the biological carbon pump between a net sink and source of CO_2 to the atmosphere (Cloern 1996). The succession in phytoplankton is~~, which is~~ intricately linked to changes in nutrient concentrations (Behrenfeld et al., 2004), temperature (Claquin et al., 2008) and light (Anning et al., 2000). More recently, the contribution of picophytoplankton to carbon export has been revaluated to show that it is proportional to their net primary production despite their small size (Richardson & Jackson, 2007). Both in the Global Ocean and the North East Atlantic, *Synechococcus* sp. are strongly associated with export flux of carbon to de~~e~~pth and are commonly found in aggregates found in trap samples in the deep ocean (Waite et al., 2000; Guidi et al., 2016). Future changes in ocean acidification and de- or eutrophication to shelf seas could impact the local phytoplankton succession and therefore carbon flow through the ecosystem (Flynn et al. 2015). The effect of changes in phytoplankton community structure on photo-physiology can often be greater than the effect of variations in nutrients (Chauton et al. 2004). To fully understand the impact that succession in phytoplankton community structure has on photosynthesis, it is important to characterise in detail coincident changes in phytoplankton size, structure and photo-physiology over many years to build up a climatological perspective of how these parameters are coupled.

While phytoplankton size and community structure are of vital importance to understanding the pelagic environment, they are difficult to measure. Phytoplankton populations in the field rarely, if ever, consist of monocultures of a single size. For scaling up from individual cells to ecosystem structure, it is important to characterise the range in

phytoplankton size and its succession under dynamic changes in hydrographic conditions which modulate community structure (Margalef, 1978).

Enumeration of phytoplankton community structure by light microscopy has traditionally provided the necessary data to assess successional changes, however this can be prohibitively time consuming and costly (Nair et al., 2008). In addition, it is not possible to accurately determine both nano and picophytoplankton using conventional light microscopy. A number of alternative approaches to estimating both phytoplankton community size and structure have been derived to provide rapid quantification of phytoplankton community dynamics. These include~~ing~~ Flow Cytometry for enumerating cell sizes of 1 to 20 µm (Moore et al., 2009), Flow Cytometer And Microscope (FlowCAM) which is an automated technique that combines both flow cytometry and microscopy (Sieracki et al. 1998) and~~,~~ imaging FlowCytobot (IFCB) which combines video and flow cytometric technology to capture images of nano and microphytoplankton over the size range from 10 to >100 µm (Olson et al. 2003). Each method has it~~'~~s merit or disadvantage (Alvarez et al. 2011, 2014, Garmendia et al. 2013, Jakobsen and Carstensen 2011), and even though they have been deployed for >20 yrs they still do not represent a direct replacement for microscopy.

Alternatively, indirect measurements of size can be made by identifying phytoplankton taxonomic groups using fluorescence *in-situ* hybridisation (FISH) probes (Groben et al., 2004), or accessory pigment concentrations as measured using high performance liquid chromatography (HPLC). Reliable means of estimating phytoplankton size and community structure from optical proxies potentially represent a quick and reliable technique to decipher changes in succession. Changes in phytoplankton signatures, ratios or clusters have been used to evaluate a wide range of ecosystem processes including changes in size classes and production (Brewin et al., 2017), export of biomass from the photic zone (Guidi et al. 2009) and the effects of environmental forcing on microbial structure (Riegmann

& Kraay 2001; Lohrenz et al. 2003). Such techniques can also be applied to remotely-sensed ocean colour data (Uitz et al. 2008). Alternative measurements of phytoplankton size can also be obtained from the specific absorption coefficient of phytoplankton (e.g. Roy et al., 2011).

In this paper we apply optical proxies to a large dataset comprising ~1500 samples from the North West Atlantic shelf, to identify successional trends in phytoplankton size and community structure. Unsupervised hierarchical cluster analysis on phytoplankton pigment data, in conjunction with absorption coefficients to estimate size-class, are used to characterise seasonal trends in photosynthetic parameter during the succession of different phytoplankton assemblages.

2. Material and methods

2.1. Study area.

The study is based on data from a large number of cruises from the North West Atlantic Shelf Province, as defined by Longhurst et al. (1995). The stations sampled were between 21.8 ºN to 62.2 ºN, 40 to 65 °W and with the majority from 43.2 ºN to 48.6 ºN. These data~~, and~~ were collected over 8 years from 1997 to 2005 in March 1996, 1999; April 1997, 1998, 2000, 2003; May 1996, 1997, 2000; June 1997, 1998, 1999, 2000, 2001, 2002; July 1998, 1999, 2002, 2003; August 2003; September 1996; October 1996, 1997, 1999, 2000, 2001, 2002; November 1997, 1999, 2001; December 2002, 2003. The number of samples analysed per day over a yearly cycle is given in Robinson et al. (2018; see Fig. 2). Data was also obtained for the polar regions, the Westerlies Domain and the Trade Winds Regime (Fig. 1). ~~The stations sampled were between 21.8 ºN to 62.2 ºN, 40 to 65 °W and with the majority from 43.2 ºN to 48.6 ºN.~~ A total of 1398 samples were analysed for the determination of HPLC phytoplankton pigments, of these 1385 samples were analysed for phytoplankton absorption

coefficients (a_{ph}) and photosynthesis-irradiance (PE) curves were determined on 726 of the samples.

2.2. Sampling regime.

Vertical profiles of temperature were obtained from CTD casts. Water samples were obtained using Niskin bottles from the surface to a maximum depth of 170 m, with 95% from depths of 50 m or less for measurements of biological, physiological and optical properties of phytoplankton. From the 1398 samples collected, 945 were from <10 m depth.

2.3. Derivation of in water properties from climatology.

Hydrographic Temperature and photosynthetically-active radiation (PAR) were measured on each cruise. C~~, but c~~limatologicaly~~~~ data from MODIS-Aqua ~~the World Ocean Atlas (WOA)~~ were~~as~~ used to generate daily PAR (which is not available from point measurements) and from the World Ocean Atlas (WOA) for the stratification index using a reference depth of 100m which was sufficiently deep that the inter-annual variability will be small. The stratification Index was calculated from:

$$\delta S = (T_s - T_{100}) / (100 - z_s) \quad (2)$$

Where δS is the stratification index, T_s is the temperature of a sample, T_{100} is the climatological temperature at of the sample at 100m, and z_s the depth of the sample.

Average surface irradiance was estimated using MODIS-Aqua monthly climatology (OceanColour level 3) which was combined with estimates of the vertical attenuation coefficient from Chl *a* from Platt et al. (2003) to obtain estimates of PAR within the mixed layer. Linear interpolation was used to derive estimates of daily irradiance from the monthly climatology. Mixed-layer depths, temperature (Locarnini et al. 2009), and salinity (Antonov

et al. 2010) were taken from WOA and potential density was taken from Jackett et al. (2006).

2.4. Analysis of phytoplankton pigments by High Performance Liquid Chromatography.

~~Chlorophyll-*a* (~~Chl *a*~~)~~ and accessory pigment concentrations were measured using HPLC following the procedure of Head & Horne (1993). Water samples were filtered onto GF/F filters before being either analysed immediately or flash frozen in liquid nitrogen at -80°C until analysis. Frozen filters were homogenised in 1.5 ml of 90% acetone, centrifuged and diluted with 0.5 M ammonium acetate at a ratio of 2:1 before being run on a Beckman C18 reverse-phase, 3 µm Ultrasphere column (Sathyendranath et al., 2005). Pigment peaks were identified for ~~chlorophyll-*a* (~~Cehl-*a*~~)~~, divinyl chlorophyll-*a* (DVchl-*a*), chlorophyll-*b* (chl-*b*), (including divinyl chlorophyll-*b* (DVchl-*b*) and monovinyl chlorophyll-*b* (MVchl-*b*), combined chlorophyll-*c1* (chl-*c1*) and chlorophyll-*c2* (chl-*c2*), chlorophyll-*c3* (chl-*c3*), peridinin (per), 19'-butanoyloxyfucoxanthin (19'-but), 19'- hexanoyloxyfucoxanthin (19'-hex), fucoxanthin (fuc), violaxanthin (viola), diadinoxanthin (diad), alloxanthin (allo), diatoxanthin (diat), zeaxanthin (zea), and β-carotene. Samples lacking any of the 17 pigments mentioned above were discarded from the analysis, leaving a total of 1397 samples that were used out of a total of 2950 samples.

2.5. Absorption coefficient of phytoplankton (a_{ph}).

Particulate absorption samples were collected on GF/F filters, and analysed as described in Stuart et al. (1998, 2000). Absorption by particulate matter ($a_p(\lambda)$) on wetted filters was measured between 400 and 750 nm relative to a blank saturated in filtered seawater, using a dual-beam Shimadzu UV-2101 PC scanning spectrophotometer with an integrating sphere (Stuart et al. 2000). Optical density measurements were divided by the geometrical path length (volume filtered divided by the clearance area of the filter) and multiplied by a factor of 2.3 to convert from decimal to natural logarithms. Detrital

absorption, $a_d(\lambda)$, was estimated following the method of Kishino et al. (1985), as modified by Stuart et al. (1998). Pigments were extracted using 20 ml of a 6:4 (vol:vol) 90% acetone and dimethyl sulfoxide (DMSO), followed by 10 ml of filtered seawater to remove any residual solvents (Stuart et al. 1998), before the absorption by the extracted filters was measured. Since water-soluble phycobiliproteins are not readily extracted using this method, a correction was applied to avoid underestimation of the absorption by phytoplankton. The detrital absorption spectrum was deconstructed into a series of Gaussian curves superimposed onto an exponential curve at the wavelengths of the peak absorption by the non-extracted pigments (420 and 666 nm for phaeopigments and 510, 550 and 590 nm for the biliproteins). The Marquardt-Levenberg algorithm was used to determine the parameters which minimise the sum of squares between the estimated and observed variables, giving a very good fit ($R^2 \sim$ 0.99), before using the fitted exponential as the measure for detrital absorption. Absorption coefficients were calculated by subtracting the optical density at 750 nm from all other wavelengths, dividing by the geometrical path length (volume filtered divided by the clearance area of the filter) and adjusting for path length amplification due to scattering by the filter. Absorption by phytoplankton was calculated by subtracting $a_d(\lambda)$ from $a_p(\lambda)$. The mean Chl *a*-specific absorption coefficient ($\bar{a}^*_{ph}$) was calculated by taking an average for all values of a_{ph} between 400 and 700 nm and dividing by ~~the~~ Chl *a* ~~concentration measured by HPLC~~.

2.6. Mean equivalent spherical diameter (MESD).

The methods of Roy et al. (2011) were used to estimate MESD from measurements of a_{ph} and pigment concentrations from HPLC. When approximated to homogeneous spheres, the absorption characteristics of the cell are a function of the concentration of pigments and the cell diameter. Due to the packaging effect, the absorption coefficient for a given

concentration of pigment in solution is greater than when it is contained within discrete particles (Duysens 1956). Chl *a* is responsible for almost all the absorption at 676 nm. Since the Chl *a* concentration in the samples is known, the degree of packaging can be calculated by comparing the absorption by phytoplankton cells at 676 nm with the estimated absorption at 676 nm from the same Chl *a* concentration using a hypothetical solution (Fig. 3). A lookup table was then used to convert this measure of packaging into MESD. The table generates values of ρ, which is the ratio between the light absorbed by a cell and the light incident on it, for a given diameter *(d)* ranging from 0 to 500 μm, to enable approximate values for *d* to be calculated. See Roy et al. (2011) for further details.

2.7. Photosynthesis-Irradiance (PE) parameters

The protocol for the determination of *PE* parameters is described in Irwin (1990), Kyewelganga et al. (1997) and Bouman et al. (2005). Seawater samples were collected at the surface and at the chlorophyll maximum based on the *in vivo* fluorescence profile obtained from CTD casts. Thirty bottles were inoculated with 185 to 370 kBq (5 to 10 μCi) of ^{14}C-labelled bicarbonate and incubated for 2-3 hours. After the incubation, the seawater was filtered through 25 mm glass fibre filters (Whatman GF/F) at a vacuum pressure of < 200 mm Hg. The filters were exposed to concentrated HCl fumes to remove any inorganic carbon present, immersed in scintillation cocktail and the disintegration time per minute of ^{14}C was counted on a liquid scintillation counter. The *PE* parameters, P_m^B and α^B, were estimated by fitting the data to the model of Platt et al. (1980). The quantum yield of photosynthesis (φ_m) was calculated as:

$$\varphi_m = 0.0231\, \alpha^B / \bar{a}^*_{ph\,(400\text{-}700)} \qquad (3)$$

where $\bar{a}^{*}_{ph\,(400\text{-}700)}$ is the mean Chl *a*-specific absorption coefficient of phytoplankton, between 400 and 700 nm, and the constant 0.0231 in the numerator converts grams to moles and hours to seconds.

2.8. Statistical analysis

To examine physiological and ecological trends of phytoplankton communities, hierarchical cluster analysis was deployed using HPLC indicator pigment data and Ward's minimum variances clustering (Fig. 2).

This is an agglomerative procedure where initially all points are considered singly, and merged in such a way to minimise the error sum of squares. The number of clusters was determined as the point where adding extra clusters caused the error sum of squares to increase. The analysis was implemented in the statistical software R via the function "hclust" as part of the "stats" package 2.5.1 (http://cran.r-project.org). Effects of variations in total biomass were eliminated by using chlorophyll-normalised pigment concentrations. Data were plotted using package "ggplot2" version 0.8.9, and mapping package "Ocean data view" version 4. To run the cluster analysis it is necessary to have all pigments present in the sample, even at low concentrations, for the full matrix to be computed. Trends between phytoplankton community clusters, MESD, photosynthetic rates and environmental parameters were visualised as running averages and analysed using linear regressin using 'R'.

3. Results

3.1. Classification of phytoplankton communities.

Ward's minimum variance hierarchical clustering was used to classify the phytoplankton communities. The technique was applied to phytoplankton pigment concentrations normalised to Chl *a*, which characterised 8 principal clusters (Fig. 2) with distinctive pigment

signatures (Fig. 3) size ranges (Fig. 4) *PE* parameters, and temperature and stratification indices (Fig. 5). Clusters 2 and 6 had the highest Chl *a* and fucoxanthin per unit Chl *a*, the largest mean cell size, P_m^B and the water masses associated with these clusters had the lowest mean temperature and stratification index. These clusters correspond with spring diatom populations (Fig. 3). Cluster 1 also had a relatively high fucoxanthin per unit Chl *a* *c*oncentration, though the mean equivalent spherical diameter (MESD) was lower than for cluster 2 and 6 (Fig. 4). This cluster represents a mixed assemblage of diatoms and prymnesiophytes. The phytoplankton community associated with Cluster 3 had a small mean cell size, with moderate to high zeaxanthin per unit Chl *a*, high α^B and low φ_m values, which is indicative of picophytoplankton. Cluster 4 phytoplankton assemblage had high zeaxanthin and Chl *b* per unit Chl *a* indicative of picophytoplankton, the lowest MESD and φ_m, high P_m^B and the water mass associated with this cluster also had a high mean mixed-layer PAR. Cluster 4 also had high concentrations of DVchl-*a* which is a key indicator of *Prochlorococcus*. Cluster 5 occurred when PAR was low and is characterised by high concentrations of Chl *b*, Chl *c*, 19'-hex, 19'-but, β-carotene per unit Chl *a*, which is indicative of flagellates. Clusters 7 and 8 occurred during high stratification, and were characterised by high concentrations of alloxanthin per unit Chl *a*, indicating the presence of cryptophytes or photosynthetic ciliates such as *Mesodinium* spp.. Cluster 8 also had very high levels concentrations of peridini~~u~~m per unit Chl *a*.

3.2.Seasonal succession in Phytoplankton communities and size.

In early spring when the stratification index was low, clusters 6 and 2 were the most abundant and are~~,~~ indicative of diatom blooms ~~, were the most abundant~~ (Fig. 6). Both of these communities then declined from Julian day 150 onwards when the stratification index

281 increased and pico and nanoeukaryote assemblages, represented by clusters 3 and 4, became
282 dominant (Fig. 6). During this period, cluster 1, the mixed assemblage of diatoms and
283 prymnesiophytes, was also present. By Julian day 250, clusters 3 and 4 decreased rapidly and
284 cluster 1 also declined and the dinoflagellate-dominated cluster 8 became more abundant. By
285 Julian day 275 these assemblages were replaced by flagellates dominated clusters 5 and 7,
286 which peaked on Julian day 300 and then declined by day 325, when the phytoplankton
287 comprised a mixed assemblage of clusters 1, 3, 4 and 8. By winter around Julian day 350, as
288 the stratification index became lower, clusters 3 and 4 decreased again, while cluster 5
289 reappeared (Fig. 6).

290 MESD was the highest in spring, decreased during the summer months, and then
291 increased again in the autumn, though not to the same extent as in spring (Fig. 7c). Over all
292 seasons, there was a significant positive correlation between MESD and total Chl *a* ($F_{1,1391}$ =
293 570, $R^2 = 0.29$, $p < 0.0001$; data not shown) and a significant negative correlation with the
294 photosynthetic parameters (Table 3). There was also a significant negative correlation
295 between MESD and temperature ($F_{1,1052} = 259.5$, $R^2 = 0.20$, $p < 0.0001$; Fig 7a, Table 3) and
296 the stratification index ($F_{1,1051} = 176$, $R^2 = 0.14$, $p < 0.0001$; Fig 6b, Table 3).

297 *3.3.Seasonal succession in photosynthetic rates.*

298 During spring, clusters 3 (pico & nanoeukaryotes), 4 (pico & nanoeukaryotes) and 7
299 (flagellates) had the highest P_m^B (3, 3 and 3.5 mg C mg Chl a^{-1} hr^{-1}, respectively; Fig. 8a).
300 During this period there seemed to be an anti-correlation with the dominant community since
301 these clusters were in low abundance. In spring, clusters 1, 2 and 6 (all diatom dominated
302 communities) were the most abundant but had the lowest P_m^B (<2, 2.5 and <1.5 mg C mg Chl
303 a^{-1} hr^{-1}, respectively). By July (JD 210), clusters 4 and 7 continued to have the highest P_m^B
304 values, which had increased to 5 and 4 mg C mg Chl a^{-1} hr^{-1}, respectively. Clusters 1 and 2

continued to have the lowest P_m^B values which had also increased slightly to 2.2 and 2.7 mg C mg Chl a^{-1} hr^{-1}, respectively. By September (JD270), clusters 4 and 7 reached their P_m^B maxima (6.6 and 5.9 mg C mg Chl a^{-1} hr^{-1}, respectively) and for clusters 5 (flagellates) and 8 (dinoflagellates), P_m^B values were >4.2 mg C mg Chl a^{-1} hr^{-1}. During this period, cluster 3 reached the lowest P_m^B values (<1.5 mg C mg Chl a^{-1} hr^{-1}). During the winter (JD360), cluster 5 had the highest values (>6 mg C mg Chl a^{-1} hr^{-1}) and cluster 1, which dominated the biomass, also reached its highest P_m^B (4 mg C mg Chl a^{-1} hr^{-1}; Fig. 8a).

For α^B in spring, all clusters exhibited similarly low values (0.01 – 0.03 mg C (mg Chl $a)^{-1}$ h^{-1}), with cluster 6 having slightly lower values and cluster 4 having higher values compared to the overall mean (Fig. 8b). From spring to summer, there was an increase in α^B associated with each cluster which reached a peak in later summer. α^B then started to diverge in June (JD170) when cluster 5 had the lowest values and cluster 7, the highest. α^B continued to diverge in late summer (JD270) when clusters 1 & 7 were between 0.06 & 0.08 mg C (mg Chl $a)^{-1}$ h^{-1}, whereas clusters 3 & 8 only reached 0.02 mg C (mg Chl $a)^{-1}$ h^{-1} (Fig. 8b). Similarly, φ_m was low in spring and increased in summer when clusters 5 and 8 reached maximum values (Fig. 8c).

P_m^B and α^B were lower when MESD was high when clusters 1, 5 and 7 dominated, and were highest as MESD decreased when clusters 2, 3, 4 and 6 dominated (Fig. 7b, d). By contrast, φ_m exhibited the opposite trend and was higher when MESD was high and lower as MESD decreased (Fig. 7f). Similarly, P_m^B and α^B increased with increasing temperature and stratification index up to 20 °C and 0.1 stratification index when clusters 2, 3, 4 and 6 dominated (Fig. 9a, b). For all data, there were significant relationships between P_m^B and α^B and temperature, stratification index and PAR (Table 3). φ_m showed a slightly different pattern with a peak both in spring at ~2 °C, when the water column was still mixed, and in

summer at 12 °C when the stratification index was 0.1 (Fig. 9g, h). Though there was a significant correlation between φ_m and PAR, there was no significant correlation between φ_m and temperature and stratification index (Fig. 9c, f, i, Table 3). .

4. Discussion

4.1. Phytoplankton community classification, size, succession and seasonality using bio-optical proxies.

Microscopy has been routinely used to characterise and enumerate phytoplankton since the 1950's (Utermöhl, 1958). Using this technique alone, very small phytoplankton (<3 μm) can be difficult to identify. Flow cytometry has therefore been deployed to identify small size phytoplankton (e.g. Moore et al., 2009). More recently, DNA and 18S rRNA probes have been used to quantify the abundance of picophytoplankton (e.g. Lie et al. 2014, Orsi et al. 2018). Signatures of phytoplankton pigments have also been used since the 1990's to elucidate the community structure of phytoplankton (e.g. Mackey et al. 1998). Automated HPLC allows for the rapid processing of pigments to determine phytoplankton groups, and a number of techniques have been developed to determine phytoplankton taxa from pigment signatures including CHEMTAX and pigment clusters (Mackey et al., 1998). In coastal waters there is generally good agreement between microscopy and HPLC pigment methods to derive phytoplankton community structure (Mackey et al. 1998). In Open Ocean oligotrophic waters, there was good agreement between the two techniques in the upper ocean, but disagreement between the two methods in deeper water samples has been reported due to depth-dependent changes in cellular pigment content and accessory pigment-to-chlorophyll ratios (Andersen et al. 1996). Brewin et al. (2014) compared HPLC and size fractionated filtration methods of deriving different phytoplankton groups and found that HPLC methods

353 tended to under-estimate Chl *a* of picoplankton and over-estimate Chl *a* of
354 nanophytoplankton compared to size filtration methods.

355 Lohrenz et al. (2003) used phytoplankton pigments to characterize size structure and
356 community composition in relation to different water masses in Chesapeake Bay, USA and
357 found that high salinity water was associated with hHaptophytes and dinoflagellates and low
358 salinity water was associated with large diatoms. Similarly, Hill et al. (2005) used pigment
359 ratios to identify successional trends in phytoplankton assemblages and found that large-sized
360 fucoxanthin containing phytoplankton were associated with the higher primary production.
361 None of these studies have used time series of phytoplankton pigments to elucidate
362 climatological changes in community structure.

363 The successional trends that we observed are consistent with previous studies in the
364 North Atlantic Ocean (Barlow et al., 1993, Lochte et al., 1993, Li 2002, Bouman et al., 2003).
365 We found that MESD is large during spring, which is associated with high concentrations of
366 fucoxanthin, predominantly from clusters 2 and 6, implying diatom dominance, when
367 stratification is absent (Fig. 8), which has also been observed by Dandonneau & Niang
368 (2007). Clusters 2 and 6 appear almost identical in terms of size, with the only visible
369 difference being the higher concentration of β-carotene in cluster 6. β-carotene plays an
370 important role in photo-protection (Llewellyn et al., 2005), but mean mixed-layer PAR was
371 higher for cluster 2 compared to cluster 6. Chlorophyll-normalised β-carotene concentrations
372 can be highly variable between different diatom species grown at the same irradiance (Dimier
373 et al. 2007), which may partially explain this trend. There was a successional change from
374 diatoms (Clusters 2 and 6) to a mixed assemblage of diatoms and prymnesiophytes (Cluster
375 1), followed by small eukaryotes with high concentrations of 19'-hex and 19'-but (Clusters 3
376 and 4) to nanoflagellates identified by Clusters 5 and 7 and finally dinoflagellates (Cluster 8).
377 Cluster 1 had a lower MESD and very high chl-*a*-normalised concentrations of chl-*c1*, *c2* and

c3 unlike the other two fucoxanthin-dominated clusters (2 and 6), though there were no differences in the degree of stratification between these clusters. This decrease in MESD as the season progressed has also been observed in the seasonal succession of this and similar areas (Margalef 1978; Barlow et al., 1993; Lochte et al., 1993; Savidge et al., 1995; Irigoien et al., 2004; Llewellyn et al., 2005). The most difficult part of the annual succession to characterise using diagnostic pigments is the transition from diatoms to prymnesiophytes, which can both contain fucoxanthin. For Cluster 1, the association of fucoxanthin with chlorophylls-*c1, c2* and *c3* is more indicative of *Phaeocystis* than diatoms (Vaulot et al., 1994). –In addition, there were 2 clusters identified with similar picophytoplankton populations. Cluster 3 is characterised by pico and nanoeukaryote pigment signatures. Cluster 4 has more cyanobacterial lineages as indicated by the presence of divinyl chlorophylls and zeaxanthin. This shift in picophytoplankton community structure across oceanographic has been reported more widely in global datasets (e.g. Bouman et al. 2011).

4.2. Coupling between phytoplankton clusters, photosynthetic rates and environmental parameters.

An increasingly accepted paradigm is that marine phytoplankton communities are formed from a background of smaller cells to which larger cells are added under conditions favourable for growth, which increases Chl *a* and PP (Chisholm,1992; Li, 2002). In the reverse direction, when the phytoplankton community becomes dominated by smaller cells, Chl *a* and PP tend to decrease. The classic theory is that winter mixing followed by stratification often results in high Chl *a*, photosynthetic rates and primary production associated with microphytoplankton dominated by diatoms (Sverdrup, 1957). As stratification intensifies, PAR and temperature also increase, but nutrients tend to decrease.

~~and~~ T~~t~~he phytoplankton community then becomes dominated by nano and picophytoplankton, resulting in a decrease in Chl *a*, photosynthetic rates and primary production (Beardall et al. 2009). This has been shown in the North Atlantic, during the progression of the spring bloom from diatoms to flagellates which is associated with lower maximum photochemical quantum efficiency and higher absorption cross section of photosystem II~~, which~~ and corresponds with a decrease in cell size, a decrease in nutrients and increasing stratification (Moore et al. 2005). Similarly in the upwelling regions off Baja California and the NW Iberian Peninsula, periods of high stratification are associated with a decrease in photosynthetic rates and primary production (Gomez-Ocampo et al., 2017; Tilstone et al., 2003).

A dichotomy exists around the community structure, cell size and the rate with which carbon is transferred through the ecosystem. Since smaller celled phytoplankton have a higher surface to volume ratio than larger cells, they have a greater ability to take up nutrients and absorb light, which could result in a higher photosynthetic efficiency (Cermeno et al., 2005). Under high nutrient concentrations and light however, large sized phytoplankton can attain higher Chl *a* normalized photosynthetic rates than smaller phytoplankton (Legendre et al. 1993; Tamigneaux et al. 1999), which suggests a higher physiological efficiency compared to smaller cells (Cermeno et al., 2005). There are an increasing number of studies however, that report an increase in photosynthetic rates and primary production during high stratification when nano and picophytoplankton dominate. In the North Pacific Subtropical Gyre for example, climate warming is associated with a shift in phytoplankton communities towards nano eukaryotes, and an increase in both Chl *a* and primary production even though dissolved silicate and phosphate have decreased (Karl et al. 2001). Similarly, in the Bay of Biscay, P_m^B is reported to be higher at the surface during summer when picophytoplankton dominate, which are positively correlated with stratification (Moran, 2007) and higher P_m^B

was correlated with low diatom abundance (Moran and Sharek, 2015). By comparison, during cruises in spring and summer, PP decreased with increasing vertical stratification in the Mediterranean Sea (Estrada et al. 2014), but the relationship could be negative (during March), positive (during March and May) or non-existent (during September) depending on the time of year. Morán and Estrada (2005)~~,~~ reported that average ~~P^B_m~~ P^B_m increased from winter to late-spring and summer, which was caused primarily by a change in the phytoplankton composition from relatively large to small cells. For all data, we found positive and significant correlations between P^B_m, α^B and temperature and stratification index indicating that in the NW Atlantic photosynthetic rates increase with temperature and water column stratification.

The variability in photosynthetic rates seems to be regional. For example, d~~D~~iatoms are reported to have the highest photosynthetic rates especially in upwelling zones due to replete light and nutrients (Babin, et al., 1996; Lorenzo, et al., 2005). In the open ocean, filamentous and colonial cyanobacteria, that have the ability to fix nitrogen, are also reported to have high photosynthetic rates (Li et al., 2011). Picophytoplankton is also reported to have high photosynthetic rates in some coastal and shelf seas (deMadariaga & Joint, 1994; Barnes, et al., 2014; Moran & Sharek, 2015; Platt et al., 1983).

In our analysis in the NW Shelf waters of the Atlantic, we found that pico and nanoeukaryotes had the highest photosynthetic rates and diatom dominated communities had the lowest rates. This is similar to the findings of Tilstone et al. (1999) in the NW Iberian Peninsula who showed that although microphytoplankton dominate the phytoplankton community, the highest and most variable photosynthetic rates are~~is~~ due to nanophytoplankton. In a temperat~~ur~~e coastal ecosystem, Xie et al. (2015) showed that the succession from nanoeukaryotes (including *Phaeocystis* sp.) to dinoflagellates resulted in an

increase in photosynthetic rates that is also associated with changes in temperature and nutrient regimes. By contrast, Mangoni et al. (2017) found in the Ross Sea that a diatom community dominated by *Pseudo-nitzschia* spp. had the highest photosynthetic- rates whereas haptophytes had lower rates. Other studies have shown that small and subtle changes in phytoplankton community composition can result in high variability in photosynthetic rates. For example, Segura et al. (2013) found that in the Argentine Sea high variability in bio-optical and photosynthetic parameters due to adaptation to heterogeneous and highly dynamics environmental conditions. A community dominated by dDiatoms and coccal cells had the highest photosynthetic rates, whereas dDiatoms and *Emiliana huxlyei* had significantly lower rates.

All clusters except cluster 5 displayed positive relationships between φ_m and size (Fig 8a), indicating higher photosynthetic efficiency as size increases, possibly due to compensation for a decrease in the efficiency of light-harvesting. It could also be the result of larger values in MESD associated with high nutrient concentrations, which can increase φ_m (Babin et al., 1996). This contrasts with the findings of Geider & Osborne (1986) who observed no variation in φ_m in relation to changes in light regime or species. Finkel (2001) and Ignatiades et al. (2002) also reported that φ_m decreases as cell size increases. We found a negative relationship between φ_m and mean daily mixed-layer PAR for clusters 1, 4, 7 and 8 (Fig. 9b), which could be due to an increase in the concentration of photo-protective pigments (Wilk-Woźniak et al., 2002, Babin et al., 1996). Since light absorbed by photo-protective pigments is dissipated as heat, less energy is used for carbon fixation, and so theoretically φ_m can decrease. For all data, both P_m^B, α^B and φ_m showed a significant negative correlation with PAR (Table 3), indicating photo-acclimation to low light and photo-inhibition at high irradiance. Negative relationships between mean daily PAR in the mixed layer and α^B were specifically observed for clusters 1, 4, 7 and 8 (Fig. 9f). Clusters 2, 3, 5 and 6, however,

showed no such response. The mean values for α^B in these clusters are lower than those for clusters 1, 4, 7 and 8 which did show a relationship between α^B and mean daily mixed-layer PAR (Fig. 5~~3~~, 9f). Given that the production of light-harvesting pigments is energetically costly for phytoplankton (Raven 1984, Geider et al., 1996), cells that are subjected to higher irradiances invest less energy in the synthesis of light-harvesting pigments, and α^B can become lower. Alternatively the relationships may be the result of a reduction of functional photosynthetic reaction centres due to photo-inhibition (Long et al., 1994), or nutrient stress (Babin et al., 1996).

Using this cluster technique to characterise the phytoplankton community succession, we were able to simultaneously characterise changes in size, environmental conditions and photosynthetic parameters. As proof-of-concept, a robust relationship between MESD from flow cytometry and absorption coefficients for the Scotian Shelf has been previous~~o~~ly reported in Bouman et al. (2003). P_m^B and α^B were highest when MESD was low, when nano and picophytoplankton dominated and when temperature (~20 °C) and stratification index (0.1) were high. These successional patterns in the dominant phytoplankton size-class and phenology support Margalef's (1978) mandala in terms of the relationship between turbulence and community structure. The study sheds new light on assemblages dominated by smaller cells, under warm, stratified conditions, having higher photosynthetic efficiencies, which has implications for the carbon flux on the NW Atlantic shelf.

Conclusion.

Using a dataset of HPLC phytoplankton pigments and phytoplankton absorption coefficients from the North West Atlantic, trends in phytoplankton distribution and succession were discerned. Cluster analysis on Cehl~~orophyll~~ *-a-* normalised accessory pigment concentrations revealed 8 distinct populations of phytoplankton with succession between the clusters dictated by seasonality and stratification. Fucoxanthin-dominated

clusters, indicating the presence of diatoms, dominated in spring when turbulence was high. As stratification increased, MESD decreased and picophytoplankton increased, while in autumn, the strength of stratification decreased, and flagellates increased in importance. High values of MESD were associated with high Chl *a* concentrations, and a highly mixed water-column, in early spring, while smaller cells were observed during the summer, when the water-column was strongly stratified. For all except one cluster, a significant positive relationship between MESD and φ_m was observed, reflecting greater quantum efficiency as the efficiency of light absorption decreased due to self-shading. Negative relationships were also observed between α^B and mean mixed layer PAR during high stratification. Assemblages dominated by smaller cells during warm, stratified conditions in summer, had higher photosynthetic rates.

Acknowledgements

This work was supported by a NERC Studentship to A.R. (*Studentship No.* 0711560248004) and is a contribution to the National Centre for Earth Observations Project of UK Natural Environment Research Council, and to the ESA Project on Photosynthetic Parameters of Phytoplankton from Space. G.H.T. was supported by UK Natural Environment Research Council National Capability funding for the Atlantic Meridional Transect (AMT) to Plymouth Marine Laboratory, which was also supported by near real time satellite service from the National Earth Observation Data Archive and Analysis Service. We would like to thank Jorn Bruggeman for his help in deriving the stratification indices. This is AMT contribution number 329.

References

525 Alvain, S., Moulin, C., Dandonneau, Y., Loisel, H. 2008. Seasonal distribution and
526 succession of dominant phytoplankton groups in the global ocean: A satellite view.
527 Global Biogeochemical Cycles, 22, GB3001, doi:10.1029/2007GB003154

528 Álvarez, E., López-Urrutia, Á., Nogueira, E. Fraga, S., 2011. How to effectively sample the
529 plankton size spectrum? A case study using FlowCAM. Journal of Plankton Research,
530 33,1119-1133.

531 Álvarez, E., Moyano, M., Lopez-Urrutia, A., Nogueira, E., Scharek, R. 2014. Routine
532 determination of plankton community composition and size structure: a comparison
533 between FlowCAM and light microscopy J. Plankton Res. 36(1): 170–184.
534 doi:10.1093/plankt/fbt069Andersen, R.A., Bidigare, R.R., Keller, M.D., Latasa, M.
535 1996. A comparison of HPLC pigment signatures and electron microscopic
536 observations for oligotrophic waters of the North Atlantic and Pacific Oceans. Deep-
537 Sea Research II, 43(2-3): 517-537.

538 Anning, T., MacIntyre, H.L., Pratt, S.M., Sammes, P.J., Gibb, S., Geider, R.J., 2000.
539 Photoacclimation in the marine diatom Skeletonema costatum. Limnology and
540 Oceanography 45, 1807–1817.

541 Antonov, J.I., Seidov, D., Boyer, T.P., Locarnini, R.A., Mishonov, A.V., Garcia, H.E.,
542 Baranova, O.K., Zweng, M.M. Johnson, D.R., 2010. World Ocean Atlas *2009,*
543 *Volume 2: Salinity.* U.S. Government Printing Office.

544 Babin, M., Morel, A., Claustre, H., Bricaud, A., Kolber, Z. Falkowski, P.G., 1996. Nitrogen-
545 and irradiance-dependent variations of the maximum quantum yield of carbon fixation
546 in eutrophic, mesotrophic and oligotrophic marine systems. Deep Sea Research Part I:
547 Oceanographic Research Papers, 43, 1241-1272.

548 Barlow, R.G., Mantoura, R.F.C., Gough, M.A. Fileman, T.W., 1993. Pigment signatures of
549 the phytoplankton composition in the northeastern Atlantic during the 1990 spring
550 bloom. Deep Sea Research Part II: Topical Studies in Oceanography, 40, 459-477.

551 Barnes, M., Tilstone G.H., Smyth, T.J., Suggett, Kromkamp J, Astoreca R, Lancelot C. 2014.
552 Absorption based algorithm of primary production for total and size-fractionated
553 phytoplankton in coastal waters. Marine Ecology Progress Series 504: 73-89.

554 Beardall, J., Stojkovic, S., Larsen, S. 2009. Living in a high CO2 world: impacts of global
555 climate change on marine phytoplankton, Plant Ecology & Diversity, 2: 191-205.

556 Behrenfeld, M.J., Prasil, O., Babin, M., Bruyant, F., 2004. In search of a physiological basis
557 for covariations in light-limited and light-saturated photosynthesis. Journal of
558 Phycology 40, 4–25.

559 Booth, B.C., Lewin, J., Postel, J.R. 1993. Temporal variation in the structure of autotrophic
560 and heterotrophic communities in the subarctic Pacific. Progr. Oceanogr. 32(1–4), 57–
561 99.

562 Bouman, H., Platt, T., Sathyendranath, S., Stuart, V., 2005. Dependence of light-saturated
563 photosynthesis on temperature and community structure. Deep Sea Research Part I:
564 Oceanographic Research Papers, 52, 1284-1299.

565 Bouman, H., Platt, T., Sathyendranath, S., Li, W.K.W., Stuart, V., Fuentes-Yaco, C., Maass,
566 H., Horne, E.P.W., Ulloa, O., Lutz, V., Kyewalyanga, M., 2003. Temperature as
567 indicator of optical properties and community structure of marine phytoplankton:
568 Implications for remote-sensing. Marine Ecology Progress Series, 258, 19-30.

569 Bouman, H., Ulloa, O., Barlow, R., Li, W.K.W., Platt, T., Zwirglmaier, K., Scanlan, D.J.,
570 Sathyendranath, S., 2011. Water-column stratification governs the community
571 structure of subtropical marine phytoplankton. Environmental Microbiology Reports,
572 3, 473-482.

573 Brewin, R.J., Sathyendranath, S., Lange, P.K., Tilstone, G.H. 2014. Comparison of two
574 methods to derive size-structure of natural samples of phytoplankton. Deep-Sea
575 Research I, 85: 72-79.

576 Brewin, R.J.W., Tilstone, G.H., Jackson, T., Cain, T., Miller, P.I., Lange, P.K., Misra, A.,
577 Airs, R.L., 2017. Modelling size-fractionated primary production in the Atlantic
578 Ocean from remote sensing. Prog. Oceanogr. 158: 130-149.

579 Campbell, L., Olson, R.J., Sosik, H. M., Abraham, A., Henrichs, D.W., Hyatt, C.J., Buskey,
580 E.J. 2010. First harmful Dinophysis (Dinophyceae, Dinophysiales) bloom in the U.S.
581 is revealed by automated imaging flow cytometry. J. Phycol. 46: 66-75.

582 Cermeno, P., Estevez-Blanco, P., Maranon, E., Fernandez, E. 2005. Maximum photosynthetic
583 efficiency of size-fractionated phytoplankton assessed by 14C uptake and fast
584 repetition rate fluorometry. Limnol. Oceanogr. 50: 1438–1446.

585 Chauton, M., Tilstone, G.H., Legrand, C., Johnsen, G., Graneli, E., Sakshaug, E. 2004. The
586 effect of phytoplankton community structure and nutrient status on bio-optical and
587 photo-physiological changes during a phytoflagellate bloom. Journal of Plankton
588 Research, 26(3): 315-324.

589 Chisholm, S.W., 1992. Phytoplankton size. In: P.G. Falkowski, A.D. Woodhead, eds,
590 Primary productivity and biogeochemical cycles in the sea. Springer, pp. 213-237.

591 Dandonneau, Y. Niang, A., 2007. Assemblages of phytoplankton pigments along a shipping
592 line through the North Atlantic and tropical Pacific. Progress in Oceanography, 73,
593 127-144.

594 Claquin, P., Probert, I., Lefebvre, S., Veron, B., 2008. Effects of temperature on
595 photosynthetic parameters and TEP production in eight species of marine microalgae.
596 Aquatic Microbial Ecology 51, 1–11.

597 Clark, D., Widdicombe, C. E., Rees, A. P., Woodward, E. M. S. 2016. The significance of
598 nitrogen regeneration for new production within a filament of the Mauritanian
599 upwelling system. Biogeosciences, 13, 2873–2888.

600 Cloern, J.E. 1996. Phytoplankton bloom dynamics in coastal ecosystems. A review with
601 some general lessons from sustained investigation of San Francisco Bay, California.
602 Reviews of Geophysics 34, 127–168.

603 Daniels, C.J., Poulton, A. J., Esposito, M., Paulsen, M. L., Bellerby, R., St John, M., Martin,
604 A. P. 2015. Phytoplankton dynamics in contrasting early stage North Atlantic spring
605 blooms: composition, succession, and potential drivers. Biogeosciences, 12, 2395–
606 2409.

607 Detmer, A.,Bathmann,U.,1997.Distribution patterns of autotrophic pico and nanoplankton
608 and their relative contribution to algal biomass during spring in the Atlantic sector of
609 the Southern Ocean. Deep Sea Res. II44(1–2): 299–320.

610 deMadariaga, I., Joint, I.R., 1994. Photosynthesis and carbon metabolism by sizefractionated
611 phytoplankton in the southern North Sea in early summer. Cont. Shelf Res. 14, 95–
612 311.

613 Dimier, C., Corato, F., Tramontano, F,. Brunet, C., 2007. Photoprotection and xanthophyll-
614 cycle activity in three marine diatoms. Journal of Phycology, 43, 937-947.

615 Estrada, M., Latasa, M., Emelianov, M., Gutiérrez-Rodríguez , A., Fernández-Castro, B.,
616 Isern-Fontanet, J., Mouriño-Carballido, B., Salat, J., Vidal., M. 2014. Seasonal and
617 mesoscale variability of primary production in the deep winter-mixing region of the
618 NW Mediterranean. Deep-Sea Research I, 94: 45–61.

619 Finkel, Z.V., 2001. Light absorption and size scaling of light-limited metabolism in marine
620 diatoms. Limnology and Oceanography, 86-94.

621 Flynn, K.J., Clark, D. R., Mitra, A., Fabian, H., Hansen, P.J., Glibert, P.M., Wheeler, G.L.,
622 Stoecker, D.K., Blackford, J.C., Brownlee, C. 2015 Ocean acidification with
623 (de)eutrophication will alter future phytoplankton growth and succession. Proc. R.
624 Soc. B 282: 20142604. http://dx.doi.org/10.1098/rspb.2014.2604

625 Garmendia, M., Revilla, M., Zarauz, L. 2013. Testing the usefulness of a simple automatic
626 method for particles abundance and size determination to derive cost-effective
627 biological indicators in large monitoring networks. Hydrobiologia, 704: 231-252.

628 Geider, R., Osborne, B., 1986. Light absorption, photosynthesis and growth of *Nannochloris*
629 *atomus* in nutrient-saturated cultures. Marine Biology, 93, 351-360.

630 Geider, R.J., Macintyre, H.L., Kana, T.M., 1996. A dynamic model of photoadaptation in
631 phytoplankton. Limnology and Oceanography, 1-15.

632 Gomez-Ocampo, E., Durazo, R., Gaxiola-Castro, G. et al. 2017. Effects of the interannual
633 variability of water column stratification on phytoplankton production and biomass at
634 the north zone off Baja California. Ciencias Marinas, 43: 109-122.

635 Groben, R., John, U., Eller, G., Lange, M., Medlin, L., 2004. Using fluorescently-labelled
636 rRNA probes for hierarchical estimation of phytoplankton diversity - a mini review.
637 Nova Hedwigia, 79, 313-320.

638 Guidi, L., Stemmann, L., Jackson, G. A., Ibanez, F., Claustre, H., Legendre, L., Picheral, M.,
639 Gorsky, G. 2009. Effects of phytoplankton community on production, size and export
640 of large aggregates: A world-ocean analysis Limnol. Oceanogr., 54: 1951–1963.

641 Guidi, L., Chaffron, S., Bittner, L., Eveillard, D., Larhlimi, A., Roux, S., Darzi, Y., Audic, S.,
642 éo Berline, L., Brum, J.R., Coelho, L.P., Ignacio Espinoza, J. C., Malviya, S.,
643 Sunagawa, S., Dimier, C., Kandels-Lewis, S., Pichera, M., Poulain, J., Searson, S.,
644 Stemmann, L., Not, F., Hingamp, P., Speich, S., Follows, M., Karp-Boss, L., Boss, E.,
645 Ogata, H., Pesant, S., Weissenbach, J., Wincker, P., Acinas, S.G., Bork, P., de Vargas,
646 C., Iudicone, D., Sullivan, M.B**.,** Raes, J., Karsenti, E, Bowler, C., Gorsky1, G. 2016.
647 Plankton networks driving carbon export in the oligotrophic ocean. Nature, 532, 465-
648 470. doi:10.1038/nature16942

649 Head, E.J.H., Horne, E.P.W., 1993. Pigment transformation and vertical flux in an area of
650 convergence in the North Atlantic. Deep Sea Research Part II: Topical Studies in
651 Oceanography, 40, 329-346.

652 Hill, V., Cota, G., Stockwell, D. 2005. Spring and summer phytoplankton communities in the
653 Chukchi and Eastern Beaufort Seas. Deep-Sea Research II, 52(24-26): 3369-3385.

654 Ignatiades, L., Psarra, S., Zervakis, V., Pagou, K., Souvermezoglou, E., Assimakopoulou, G.,
655 Gotsis-Skretas, O., 2002. Phytoplankton size-based dynamics in the Aegean Sea
656 (Eastern Mediterranean). Journal of Marine Systems, 36, 11-28.

657 Irigoien, X., Flynn, K. J., Harris, R. P. 2005. Phytoplankton blooms: A 'loophole' in
658 microzooplankton grazing impact? J. Plankt. Res. 27: 313–321.

659 Irwin, A.J., Finkel, Z.V., Schofield, O.M.E., Falkowski, P.G., 2006. Scaling-up from nutrient
660 physiology to the size-structure of phytoplankton communities. Journal of Plankton
661 Research, 28, 459-471.

662 Jakobsen, H. H., Carstensen, J. 2011. FlowCAM: Sizing cells and understanding the impact
663 of size distributions on biovolume of planktonic community structure. Aquat Microb
664 Ecol., 65: 75–87, doi: 10.3354/ame01539

665 Jackett, D.R., Mcdougall, T.J., Feistel, R., Wright, D.W., Griffites, S.M., 2006. Algorithms
666 for density, potential temperature, conservative temperature, and the freezing
667 temperature of seawater. Journal of Atmospheric and Oceanic Technology, 23, 1709.

668 Jiang, L., Schofield, O.M., Falkowski, P.G., 2005. Adaptive evolution of phytoplankton cell
669 size. American naturalist, 496-505.

670 Karl, D.M., Bidigare, R.R., Letelier, R.M. 2001. Long-term changes in plankton community
671 structure and productivity in the North Pacific Subtropical Gyre: The domain shift
672 hypothesis. Deep-Sea Research II 48: 1449-1470.

673 Kiørboe, T., 1993. Turbulence, water column structure and phytoplankton cell size. Advances
674 in Marine Biology, 29, 1-72.

675 Kishino, M., Takahashi, M., Ichimura, S., 1985. Estimation of the spectral absorption
676 coefficients of phytoplankton in the sea. Bulletin of Marine Science, 37, 634-642.

677 Kyewalyanga, M.N., Platt, T., Sathyendranath, S. 1997. Estimation of the photosynthetic
678 action spectrum: implication for primary production models. Marine Ecology
679 Progress Series 146, 207–223.

680 Legendre, L., Gosselin, M., Hirche, H.J., Kattner, G., Rosenberg, G. 1993. Environmental
681 control and potential fate of size fractionated phytoplankton in the Greenland Sea
682 (758N). Marine Ecology Progress Series **98:** 297–313.

683 Li, W.K.W., Subba-Raio, D., Harrison, W.G., Smith, J.C., Cullen, J.J., Irwin, B., Platt,T.
684 1983.Autotrophic picoplankton in the tropical ocean. Science 219, 292–295.

685 Li, W.K.W., 2002. Macroecological patterns of phytoplankton in the northwestern North
686 Atlantic Ocean. Nature, 419, 154-157.

687 Li, B., Karl, D.M., Letelier, R.M., Church, M.J., 2011. Size-dependent photosynthetic
688 variability in the North Pacific Subtropical Gyre. Mar. Ecol. Prog. Ser. 440, 27–
689 40.Lie, A.A.Y., Liu, Z., Hu, S.K., Jones, A.C., Kim, D.Y., Countway, P.D., et al.
690 2014. Investigating microbial eukaryotic diversity from a global census: insights from
691 a comparison of pyrotag and full-length sequences of 18S rRNA genes. Appl.
692 Environ. Microbiol., 80: 4363–4373.

693 Llewellyn, C.A., Fishwick, J.R., Blackford, J.C., 2005. Phytoplankton community
694 assemblage in the English Channel: A comparison using chlorophyll a derived from
695 HPLC-CHEMTAX and carbon derived from microscopy cell counts. Journal of
696 Plankton Research, 27, 103-119.

697 Locarnini, R.A., Mishonov, A.V., Antonov, J.I., Boyer, T.P., Garcia, H.E., 2009. World
698 Ocean Atlas 2009, Volume 1, Temperature.

699 Lochte, K., Ducklow, H.W., Fasham, M.J.R., Stienen, C., 1993. Plankton succession and
700 carbon cycling at 47°N 20°W during the JGOFS North Atlantic Bloom Experiment.
701 Deep Sea Research Part II: Topical Studies in Oceanography, 40, 91-114.

702 Long, S., Humphries, S., Falkowski, P.G., 1994. Photoinhibition of photosynthesis in nature.
703 Annual review of plant biology, 45, 633-662.

704 Longhurst, A., Sathyendranath, S., Platt, T., Caverhill, C., 1995. An estimate of global
705 primary production in the ocean from satellite radiometer data. Journal of Plankton
706 Research, 17, 1245-1271.

707 Lohrenz, S.E. Carroll, C.L., Weidemann, A.D. 2003. Variations in phytoplankton pigments,
708 size structure and community composition related to wind forcing and water mass
709 properties on the North Carolina inner shelf. Continental Shelf Research, 23(14-15):
710 1447-1464.

711 Lorenzo LM, Arbones B, Tilstone GH, Figueiras F.G. 2005. Across-shelf variability of
712 phytoplankton composition, photosynthetic parameters and primary production in the
713 NW Iberian upwelling system. Journal of Marine Systems 54 (1-4): 157-173.Malone,
714 T.C. 1977. Light-saturated photosynthesis by phytoplankton size fractions in the New
715 York bight, USA. Mar. Biol. 42: 281–292.

716 Mackey, D.J., Higgins, H.W., Mackey, M.D., Holdsworth, D. 1998. Algal class abundances
717 in the western equatorial Pacific: Estimation from HPLC measurements of chloroplast
718 pigments using CHEMTAX. Deep-Sea Research I, 45(9): 1441-1468

719 Mangoni, O., Saggiomo, V., Bolinesi, F., Margiotta, F., Budillon, G., Cotroneo, Y., Misic,
720 C., Rivaro, P., Saggiomo, M. 2017. Phytoplankton blooms during austral summer in

721 the Ross Sea, Antarctica: Driving factors and trophic implications. PlosOne, 12(4):
722 e0176033. https://doi.org/10.1371/journal.pone.0176033

723 Margalef, R., 1978. Life-forms of phytoplankton as survival alternatives in an unstable
724 environment. Oceanologica acta, **134**, pp. 493-509.

725 Moore, C.M., Lucas, M.I., Sanders, R., Davidson, R. 2005. Basin-scale variability of
726 phytoplankton bio-optical characteristics in relation to bloom state and community structure
727 in the Northeast Atlantic. Deep-Sea Research I 52: 401-419.

728 Moore, C., Barnard, A., Fietzek, P., Lewis, M.R., Sosik, H.M., White, S., Zielinski, O., 2009.
729 Optical tools for ocean monitoring and research. Ocean Science, 5, 661-684.

730 Morán, X.A.G. 2007. Annual cycle of picophytoplankton photosynthesis and growth rates in
731 a temperate coastal ecosystem: a major contribution to carbon fluxes. Aquat Microb
732 Ecol. 49: 267–279.

733 Morán, X.A.G., Estrada, M. 2005. Winter pelagic photosynthesis in the NW Mediterranean,
734 Deep-Sea Research I, 52, 1806–1822.

735 Morán, X.A.G., Sharek, R., 2015. Photosynthetic parameters and primary production, with
736 focus on large phytoplankton, in a temperate mid-shelf ecosystem. Estuar. Coast.
737 Shelf Sci. 154, 255–263.

738 Morel, A., Bricaud, A. 1981. Theoretical Results Concerning Light-Absorption in a Discrete
739 Medium, and Application to Specific Absorption of Phytoplankton. Deep-Sea Res. I.
740 28, 1375-1393.

741 Munk, W.H., Riley, G.A. 1974. Absorption of nutrients by aquatic plants. J. Mar. Res.
742 11:215.

743 Nair, A., Sathyendranath, S., Platt, T., Morales, J., Stuart, V., Forget, M., Devred, E.,
744 Bouman, H., 2008. Remote sensing of phytoplankton functional types. Remote
745 Sensing of Environment, 112, 3366-3375.

746 Olson, R. J., Shalapyonok, A., Sosik, H. M. 2003. An automated submersible flow cytometer
747 for analysing pico and nanophytoplankton: FlowCytobot. Deep-Sea Research I 50:
748 301–315.

749 Orsi W.D., Wilken S., del Campo, J., Heger, T., James, E., Richards, T. A., Keeling, R. J.,
750 Worden, A.Z., Santoro, A.E. 2018. Identifying protist consumers of photosynthetic
751 picoeukaryotes in the surface ocean using stable isotope probing. Environ. Microbio.,
752 20(2), 815–827. doi:10.1111/1462-2920.14018.

753 Pahlow, M., Riebesell, U., Wolf-Gladrow, D.A. 1997. Impact of cell shape and chain
754 formation on nutrient acquisition by marine diatoms. Limnol. Oceanogr., 42, 1660-
755 1672.

756 Platt, T., Gallegos, C., Harrison, W., 1980. Photoinhibition of photosynthesis in natural
757 assemblages of marine phytoplankton. Journal of Marine Research, 38.

758 Platt, T., Rao, D.V.S., Irwin, B., 1983. Photosynthesis of picoplankton in the oligotrophic
759 ocean. Nature 301, 702–704.

760 Platt, T., Fuentes-Yaco, C K.T.F., 2003. Marine ecology: spring algal bloom and larval fish
761 survival. Nature, 423, 398-399.

762 R Core Development Team 2009. R: A language and environment for statistical computing.
763 R foundation for Statistical Computing, Vienna, Austria. ISBN 3-900051-07-0, URL
764 http://www.R-project.org

765 Raven, J.A., 1984. Physiological correlates of the morphology of early vascular plants.
766 Botanical Journal of the Linnean Society, 88, 105-126.

767 Raven, J.A., 1998. The twelfth Tansley lecture: Small is beautiful: The picophytoplankton.
768 Functional ecology, 12, 503-513. Richardson, T.L., Jackson, G.A. 2007. Small
769 Phytoplankton and Carbon Export from the Surface Ocean. Science, 315, 838-840.
770 DOI: 10.1126/science.1133471

771 Riegman, R., Kraay, G.W. 2001. Phytoplankton community structure derived from HPLC
772 analysis of pigments in the Faroe-Shetland Channel during summer 1999: the
773 distribution of taxonomic groups in relation to physical/chemical conditions in the
774 photic zone. Journal of Plankton Research, 23: 191-205.

775 Robinson, A., Bouman, H.A., **Tilstone, G.H.,** Sathyendranath, S. (2018). Size class
776 dependent relationships between temperature and phytoplankton photosynthesis-
777 irradiance parameters in the Atlantic Ocean. *Frontiers in Marine Science,* 4:435, doi:
778 10.3389/fmars.2017.00435

779 Roy, S., Sathyendranath, S., Platt, T., 2011. Retrieval of phytoplankton size from bio-optical
780 measurements: theory and applications. Journal of The Royal Society Interface, 8,
781 650-660.

782 Sathyendranath, S., Stuart, V., Platt, T., Bouman, H., Ulloa, O., Maass, H., 2005. Remote
783 sensing of ocean colour: Towards algorithms for retrieval of pigment composition.
784 Indian Journal of Marine Sciences, 34, 333-340.

785 Savidge, G., Boyd, P., Pomroy, A., Harbour, D., Joint, I., 1995. Phytoplankton production
786 and biomass estimates in the northeast Atlantic Ocean, May-June 1990. Deep-Sea
787 Research Part I: Oceanographic Research Papers, 42, 599-617.

788

789 Segura V, Lutz VA, Dogliotti A, Silva RI, Negri RM, Akselman R, Benavides H (2013) Phytoplankton
790 types and primary production in the Argentine Sea. Mar Ecol Prog Ser 491:15-31.

791 Sieracki, M.E., Verity, P.G., Stoecker, D.K., 1993. Plankton community response to
792 sequential silicate and nitrate depletion during the 1989 North Atlantic spring bloom.
793 Deep-Sea Research Part II, 40, 213-225.

794 Stuart, V., Sathyendranath, S., Head, E.J.H., Platt, T., Irwin, B., Maass, H., 2000. Bio-optical
795 characteristics of diatom and prymnesiophyte populations in the Labrador Sea. Marine
796 Ecology Progress Series, 201, 91-106.

797 Stuart, V., Sathyendranath, S., Platt, T., Maass, H., Irwin, B.D., 1998. Pigments and species
798 composition of natural phytoplankton populations: Effect on the absorption spectra.
799 Journal of Plankton Research, 20, 187-217.

800 Sverdrup, H. U. 1957. On conditions for the vernal blooming of phytoplankton. Journal du
801 Conseil International pour l'Exploration de la Mer, 18, 287–295.

802 Tamigneaux, E., Legendre, L., Klein, B., Mingelbier, M. 1999. Seasonal dynamics and
803 potential fate of size-fractionated phytoplankton in a temperate nearshore environment
804 (Western Gulf of St. Lawrence, Canada). Estuarine Coastal Shelf Science 48: 253–
805 269.

806 Tilstone, G.H., Figueiras, F.G., Fermín, E.G., Arbones, B. 1999. The significance of nano-
807 phytoplankton photosynthesis and primary productivity in a coastal upwelling
808 ecosystem (Ría de Vigo, NW Spain). Marine Ecology Progress Series 183: 13-27.

809 Tilstone, G.H., Lorenzo, L.M., Arbones, B., Figueiras, F.G. 2003. Photosynthesis primary
810 production and phytoplankton growth rates different hydrographic conditions at the
811 NW Iberian upwelling margin. Marine Ecology Progress Series, 252: 89-104.

812 Waite, A.M., Safi, K.A., Hall, J.A., Nodder, S.D., 2000. Limnol. Oceanogr. 45, 87.
813 Uitz, J., Huot, Y., Bruyant, F., Babin, M., Claustre, H., Claustre, H., 2008. Relating
814 Phytoplankton Photophysiological Properties to Community Structure on Large
815 Scales. Limnology and Oceanography, 53, 614-630.

816 Utermöhl, H., 1958. Perfeccionamento del método cuantitativo del fitoplancton. Comum.
817 Assoc. Int. Limnol. Teor. Apl. 9,1–89.

818 Vaulot, D., Birrien, J., Marie, D., Casotti, R., Veldhuis, M.J.W., Kraay, G.W., Chrétiennot-
819 Dinet, M., 1994. Morphology, ploidy, pigment composition, and genome size of
820 cultured strains of *Phaeocystis* (Prymnesiophyceae). Journal of Phycology, 30, 1022-
821 1035.

822 Wassmann, P., Ratkova, T., Reigstad, M., 2005. The contribution of single and colonial cells
823 of *Phaeocystis pouchetii* to spring and summer blooms in the north-eastern North
824 Atlantic. Harmful Algae, 4, 823-840.

825 Wickham, H., 2009. ggplot2: Elegant Graphics for Data Analysis. 2nd edn. Springer
826 Publishing Company, Incorporated.

827 Wilk-Woźniak, E., Pociecha, A., Bucka, H., 2002. Phytoplankton-zooplankton interactions,
828 size relations and adaptive responses. A short review. Ecohydrology and
829 Hydrobiology, 1, 511-517.

830 Xie Y., Tilstone G.H., Widdicombe, C., Woodward, E.M.S., Harris, C., Barnes, M.K. 2015.
831 Effects of increases in temperature and nutrients on phytoplankton community
832 structure and photosynthesis in the Western English Channel. *Marine Ecology*
833 *Progress Series* 519: 61-73. doi: 10.3354/meps11101

834

Figure Legends.

Fig. 1. Station locations in the North Atlantic used for cluster analysis of HPLC phytoplankton pigment data.

Fig. 2. Results of Ward's hierarchical cluster analysis using chlorophyll-normalised HPLC pigment concentrations. (a) Descent curve showing clear elbow at 8 clusters. (b) Dendrogram showing Euclidian distances between samples, with cluster numbers.

Fig. 32. Boxplots showing (ai) Percentage of total Cehl-*a* which is divinyl, (bj) Chl-*a* normalised chl-*b*, (ck) Chl-*a* normalised combined chl-*c1* and chl-*c2*, (dl) Chl-*a* normalised β-carotene, (em) Chl-*a* normalised chl-*c3*, (fn) Chl-*a* normalised fucoxanthin, (go) Chl-*a* normalised peridinin, (hp) Chl-*a* normalised alloxanthin, (iq) Chl-*a* normalised 19'-butanoyloxyfucoxanthin, (jr) Chl-*a* normalised 19'-hexanoyloxyfucoxanthin, (ks) Chl-*a* normalised zeaxanthin.

Fig. 43. Density plots of the size distributions of different phytoplankton populations from hierarchical cluster analysis on chlorophyll normalised HPLC pigment concentrations. Lines coloured according to cluster. Cluster 1: red, 2: green, 3: dark blue, 4: light blue, 5: purple, 6: yellow, 7: grey, 8: pink. Size structure estimated using absorption at 676nm.

Fig. 54. Boxplots showing photosynthetic parameters and chlorophyll normalised HPLC pigment concentrations for the different clusters. (a.) Total chlorophyll-*a* (µg/l), (b.) Temperature (°C), (c.) Photosynthetically active radiation (E m^{-2} d^{-1}), (d.) φ_m (E m^{-2} d^{-1}), (e.) P_m^B (mgC (mg chl-*a*)$^{-1}$ h^{-1}), (f.) α^B (mg C (mg chl-*a*)$^{-1}$ h^{-1} µmol quanta m^{-2} s^{-1})$^{-1}$, (g.) Mean equivalent spherical diameter from absorption (µm), (h.) Stratification index, defined as the difference between samples temperature and climatological prediction for the temperature at 100m / offset in depth (°C m^{-1}), (i.) proportion of divinyl Chl *a*.

Fig. 65. (a) Proportion of samples in each cluster with respect to Julian day in North West Atlantic Shelfves Province as defined by Longhurst et al. (1995). Clusters assigned using hierarchical cluster analysis on Cehl-*a* normalised HPLC pigments. (b) Proportion of samples in each cluster with respect to the degree of stratification in the North West Atlantic Shelves ~~Province as defined by Longhurst *et al.* (1995). Clusters assigned using hierarchical cluster analysis on chl-*a* normalised HPLC pigments.~~ Stratification index is defined as the difference between sample temperature and climatological prediction for the temperature at 100 m divided by the offset in depth.

Fig. 76. Relationship between mean equivalent spherical diameter and environmental and biological variables; (a.) temperature, (b.) P_m^B, (c.) Julian Day, (d.) α^B, (e.) stratification index, (f.) φ_m. Points are coloured according to phytoplankton cluster as assigned using chlorophyll normalised hierarchical cluster analysis. Cluster 1: red, 2: green, 3: dark blue, 4: light blue, 5: purple, 6: yellow, 7: grey, 8: pink. Black line is the running average of all points.

Fig. 87. Relationship between (a.) maximum photosynthetic rate (P_m^B; mg C mg Chl a^{-1} hr^{-1}), (b.) light limited slope of photosynthesis (α^B (mg C (mg chl-*a*)$^{-1}$ h^{-1} µmol quanta m^{-2} s^{-1})$^{-1}$) (c.) maximum quantum yield (φ_m (E m $^{-2}$ d $^{-1}$)) for each cluster and time of the year (Julian Day). ~~Coloured~~ Coloured liness areare the running average for each clustereach cluster.

Fig. 98. Relationship between P_m^B (mg C mg Chl a^{-1} hr^{-1}) and (a.) temperature, (b.) stratification index, (c.) mean PAR in the mixed layer (E m $^{-2}$ d $^{-1}$); α^B (mg C mg chl-*a*)$^{-1}$ h^{-1} µmol quant m^{-2} s^{-1})$^{-1}$ and (d.) temperature, (e.) stratification index, (f.) mean PAR in the mixed layer (E m $^{-2}$ d $^{-1}$); and φ_m (mol C (mol quanta)$^{-1}$), (g.) temperature, (h.) stratification index, (i.) mean PAR in the mixed layer (E m $^{-2}$ d $^{-1}$). Points are coloured according to hierarchical cluster analysis on chlorophyll normalised HPLC pigments. ~~Solid line is the best fit through all data.~~ Black line is the running average of all points.

Table 1. Summary of key cluster properties, showing sample temperature, depth, day of year, total HPLC chl-*a, PE* parameters, quantum yield (φ_m), mean-specific absorption between 350 and 700 nm ($\bar{a}^*_{ph}$). Mean phytoplankton MESD was estimated using phytoplankton absorption coefficients (Roy et al. 2011).

Table 2. Summary of pigments present in the different clusters and ecological implications.

Table 3. Statistical relationships between environmental variables and (A.) mean equivalent spherical diameter, (b.) photosynthetic rates using linear regression. R^2 is the coefficient of variation, F is the mean square to mean square error ratio, df denotes the degrees of freedom and P is the critical significance value.

~~Statistical relationships between environmental variables and (A.) mean equivalent spherical diameter, (b.) photosynthetic rates.~~

High photosynthetic rates associated with pico and nanophytoplankton communities and high stratification index on the North West Atlantic Shelf.

Alex Robinson[1], Heather Bouman[1], Gavin Tilstone[2*], Shubha Sathyendranath[2]

Research Highlights.

- Cluster analysis employed on HPLC pigments to identify trends in phytoplankton succession.
- Variability in succession, photosynthetic rates, environmental parameters assessed.
- Diatom communities had the lowest photosynthetic rates throughout the year.
- Pico & nanoplankton under warm stratified conditions had higher photosynthetic rates.

High photosynthetic rates associated with pico and nanophytoplankton communities and high stratification index on the North West Atlantic Shelf.

Alex Robinson[1□], Heather Bouman[1], Gavin Tilstone[2*], Shubha Sathyendranath[2]

[1]*Department of Earth Sciences, University of Oxford, South Parks Road, Oxford, OX1 3AN, UK.*

[2]*Plymouth Marine Laboratory, Prospect Place, West Hoe, Plymouth, PL1 3DH, UK.*

[□]*Current address: Centre for Ecology and Hydrology, MacLean Building, Benson Lane, Wallingford, Oxon, OX10 8BB, UK.*

***Corresponding author:** Dr. Gavin Tilstone, ghti@pml.ac.uk

Running title: Phytoplankton succession and photosynthesis.

KEY WORDS: Atlantic Ocean, Phytoplankton size, Phytoplankton succession, Photosynthesis Parameters.

Abstract

The biological dynamics of pelagic marine ecosystems are strongly influenced by the size structure and ecological succession of phytoplankton, which in turn modifies photosynthetic efficiency. Variability in photosynthetic rates is closely coupled with changes in community structure, but it is difficult to obtain coincident data at high enough resolution to characterise these changes. In this study, we employ hierarchical cluster analysis on chlorophyll-normalised high performance liquid chromatography (HPLC) pigment concentrations from the North West Atlantic shelf, to identify seasonal successional trends amongst phytoplankton populations. Changes in phytoplankton community were also analysed as a function of mean equivalent spherical diameter (MESD) derived from absorption measurements, photosynthetic rates, water-column stratification and temperature. Well-mixed conditions in spring to early summer were associated with populations of large cells containing high concentrations of fucoxanthin, chlorophyll-*c*1 and chlorophyll-*c*2 relative to chlorophyll-*a* (Chl *a*). As stratification increased over the course of the summer, these cells were replaced by populations dominated by chlorophyll-*b*, 19'-hexanoyloxyfucoxanthin, 19'-butanoyloxyfucoxanthin and divinyl chlorophyll-*a,* indicative of small picophytoplankton. As stratification decreased in autumn, MESD and alloxanthin increased, suggesting the presence of cryptophytes. Positive relationships were found between MESD and the quantum yield of photosynthesis (φ_m) for 7 out of the 8 phytoplankton clusters identified, while negative relationships between mean mixed layer photosynthetically active radiation and φ_m and the light limited slope of photosynthesis (α^B) were observed for 4 clusters, as a result of nutrient limitation and photo-protection. The highest photosynthetic rates were associated with a pico & nanophytoplankton communities, which increased from spring to late summer as stratification intensified. By contrast, diatom communities had the lowest photosynthetic rates throughout the year. These successional patterns in the dominant phytoplankton size-class

and phenology support Margalef's mandala in terms of the relationship between turbulence and community structure. The study sheds new light on assemblages dominated by smaller cells, under warm, stratified conditions, having higher photosynthetic efficiencies, which has implications for the carbon flux on the NW Atlantic shelf.

1. Introduction

The ecological functioning of marine phytoplankton communities is strongly influenced by the species present and their size (Chisholm 1992, Raven 1998). There are more than 5000 species in the global ocean, which have a 1000 fold range in cell size (Jiang et al., 2005). In the North Atlantic, cell size varies from ~0.6 μm to >1000 μm, which is highly correlated with seasonal changes in water column stratification (Kiørboe 1993). Large phytoplankton, especially diatoms, thrive in turbulent and partially mixed waters that are rich in nitrate, which facilitates rapid assimilation of nutrients and carbon fixation (Pahlow et al., 1997). Smaller cells that comprise the picophytoplankton, tend to inhabit nutrient poor, stratified, oligotrophic regions which are highly stratified (Munk and Riley,1974; Malone, 1977). Margalef (1978) proposed a mandala to divide phytoplankton groups according to the levels of turbulence and nutrient availability.

Phytoplankton productivity in the North Atlantic accounts for ~50% of the global ocean production (Wassmann, 1990), which has huge implications for the ocean biological carbon pump (Daniels et al., 2015). The classic theory of succession in this region is that spring bloom forms as the winter mixed-layer shoals, exposing high nutrient concentrations in the surface layers to light as incident irradiance and day length increase (Sverdrup, 1957). The spring bloom is often dominated by diatoms, which are replaced by nanophytoplankton as nutrients become depleted (Margalef, 1978). Different hydrographic circulation patterns

67 can modulate the recycling and regeneration of nutrients in the euphotic zone which can lead
68 to successional changes in pico, nano and microphytoplankton (e.g. Clarke et al. 2016). New
69 methods of detection of phytoplankton functional types from satellite data similarly illustrate
70 an annual succession between diatoms, nanophytoplankton and *Prochlorococcus* (Alvain et
71 al. 2008). These successional changes modify the biological carbon pump between a net sink
72 and source of CO_2 to the atmosphere (Cloern 1996). The succession in phytoplankton is
73 intricately linked to changes in nutrient concentrations (Behrenfeld et al., 2004), temperature
74 (Claquin et al., 2008) and light (Anning et al., 2000). More recently, the contribution of
75 picophytoplankton to carbon export has been revaluated to show that it is proportional to their
76 net primary production despite their small size (Richardson & Jackson, 2007). Both in the
77 Global Ocean and the North East Atlantic, *Synechococcus* sp. are strongly associated with
78 export flux of carbon to depth and are commonly found in aggregates found in trap samples
79 in the deep ocean (Waite et al., 2000; Guidi et al., 2016). Future changes in ocean
80 acidification and de- or eutrophication to shelf seas could impact the local phytoplankton
81 succession and therefore carbon flow through the ecosystem (Flynn et al. 2015). The effect of
82 changes in phytoplankton community structure on photo-physiology can often be greater than
83 the effect of variations in nutrients (Chauton et al. 2004). To fully understand the impact that
84 succession in phytoplankton community structure has on photosynthesis, it is important to
85 characterise in detail coincident changes in phytoplankton size, structure and photo-
86 physiology over many years to build up a climatological perspective of how these parameters
87 are coupled.

88 While phytoplankton size and community structure are of vital importance to
89 understanding the pelagic environment, they are difficult to measure. Phytoplankton
90 populations in the field rarely, if ever, consist of monocultures of a single size. For scaling up
91 from individual cells to ecosystem structure, it is important to characterise the range in

92 phytoplankton size and its succession under dynamic changes in hydrographic conditions
93 which modulate community structure (Margalef, 1978).

94 Enumeration of phytoplankton community structure by light microscopy has
95 traditionally provided the necessary data to assess successional changes, however this can be
96 prohibitively time consuming and costly (Nair et al., 2008). In addition, it is not possible to
97 accurately determine both nano and picophytoplankton using conventional light microscopy.
98 A number of alternative approaches to estimating both phytoplankton community size and
99 structure have been derived to provide rapid quantification of phytoplankton community
100 dynamics. These include Flow Cytometry for enumerating cell sizes of 1 to 20 μm (Moore et
101 al., 2009), Flow Cytometer And Microscope (FlowCAM) which is an automated technique
102 that combines both flow cytometry and microscopy (Sieracki et al. 1998) and imaging
103 FlowCytobot (IFCB) which combines video and flow cytometric technology to capture
104 images of nano and microphytoplankton over the size range from 10 to >100 μm (Olson et al.
105 2003). Each method has its merit or disadvantage (Alvarez et al. 2011, 2014, Garmendia et al.
106 2013, Jakobsen and Carstensen 2011), and even though they have been deployed for >20 yrs
107 they still do not represent a direct replacement for microscopy. Alternatively, indirect
108 measurements of size can be made by identifying phytoplankton taxonomic groups using
109 fluorescence *in-situ* hybridisation (FISH) probes (Groben et al., 2004), or accessory pigment
110 concentrations as measured using high performance liquid chromatography (HPLC). Reliable
111 means of estimating phytoplankton size and community structure from optical proxies
112 potentially represent a quick and reliable technique to decipher changes in succession.
113 Changes in phytoplankton signatures, ratios or clusters have been used to evaluate a wide
114 range of ecosystem processes including changes in size classes and production (Brewin et al.,
115 2017), export of biomass from the photic zone (Guidi et al. 2009) and the effects of
116 environmental forcing on microbial structure (Riegmann & Kraay 2001; Lohrenz et al. 2003).

117 Such techniques can also be applied to remotely-sensed ocean colour data (Uitz et al. 2008).
118 Alternative measurements of phytoplankton size can also be obtained from the specific
119 absorption coefficient of phytoplankton (e.g. Roy et al., 2011).

120 In this paper we apply optical proxies to a large dataset comprising ~1500 samples
121 from the North West Atlantic shelf, to identify successional trends in phytoplankton size and
122 community structure. Unsupervised hierarchical cluster analysis on phytoplankton pigment
123 data, in conjunction with absorption coefficients to estimate size-class, are used to
124 characterise seasonal trends in photosynthetic parameter during the succession of different
125 phytoplankton assemblages.

126

127 **2. Material and methods**

128 *2.1. Study area.*

129 The study is based on data from a large number of cruises from the North West Atlantic Shelf
130 Province, as defined by Longhurst et al. (1995). The stations sampled were between 21.8 º N
131 to 62.2 º N, 40 to 65 °W and with the majority from 43.2 º N to 48.6 º N. These data were
132 collected over 8 years from 1997 to 2005 in March 1996, 1999; April 1997, 1998, 2000,
133 2003; May 1996, 1997, 2000; June 1997, 1998, 1999, 2000, 2001, 2002; July 1998, 1999,
134 2002, 2003; August 2003; September 1996; October 1996, 1997, 1999, 2000, 2001, 2002;
135 November 1997, 1999, 2001; December 2002, 2003. The number of samples analysed per
136 day over a yearly cycle is given in Robinson et al. (2018; see Fig. 2). Data was also obtained
137 for the polar regions, the Westerlies Domain and the Trade Winds Regime (Fig. 1). A total of
138 1398 samples were analysed for the determination of HPLC phytoplankton pigments, of these
139 1385 samples were analysed for phytoplankton absorption coefficients (a_{ph}) and
140 photosynthesis-irradiance (*PE*) curves were determined on 726 of the samples.

141 *2.2. Sampling regime.*

142 Vertical profiles of temperature were obtained from CTD casts. Water samples were obtained
143 using Niskin bottles from the surface to a maximum depth of 170 m, with 95% from depths
144 of 50 m or less for measurements of biological, physiological and optical properties of
145 phytoplankton. From the 1398 samples collected, 945 were from <10 m depth.

146 *2.3. Derivation of in water properties from climatology.*

147 Hydrographic Temperature and photosynthetically-active radiation (PAR) were measured on
148 each cruise. Climatological data from MODIS-Aqua were used to generate daily PAR (which
149 is not available from point measurements) and from the World Ocean Atlas (WOA) for the
150 stratification index using a reference depth of 100m which was sufficiently deep that the
151 inter-annual variability will be small. The stratification Index was calculated from:

152 $$\delta S = (T_s - T_{100}) / (100 - z_s) \quad (2)$$

153 Where δS is the stratification index, T_s is the temperature of a sample, T_{100} is the
154 climatological temperature at of the sample at 100m, and z_s the depth of the sample.

155 Average surface irradiance was estimated using MODIS-Aqua monthly climatology
156 (OceanColour level 3) which was combined with estimates of the vertical attenuation
157 coefficient from Chl *a* from Platt et al. (2003) to obtain estimates of PAR within the mixed
158 layer. Linear interpolation was used to derive estimates of daily irradiance from the monthly
159 climatology. Mixed-layer depths, temperature (Locarnini et al. 2009), and salinity (Antonov
160 et al. 2010) were taken from WOA and potential density was taken from Jackett et al. (2006).
161 *2.4. Analysis of phytoplankton pigments by High Performance Liquid Chromatography.*

162 Chl *a* and accessory pigment concentrations were measured using HPLC following
163 the procedure of Head & Horne (1993). Water samples were filtered onto GF/F filters before

being either analysed immediately or flash frozen in liquid nitrogen at -80°C until analysis. Frozen filters were homogenised in 1.5 ml of 90% acetone, centrifuged and diluted with 0.5 M ammonium acetate at a ratio of 2:1 before being run on a Beckman C18 reverse-phase, 3 µm Ultrasphere column (Sathyendranath et al., 2005). Pigment peaks were identified for Chl-*a*, divinyl chlorophyll-*a* (DVchl-*a*), chlorophyll-*b* (chl-*b*), (including divinyl chlorophyll-*b* (DVchl-*b*) and monovinyl chlorophyll-*b* (MVchl-*b*), combined chlorophyll-*c1* (chl-*c1*) and chlorophyll-*c2* (chl-*c2*), chlorophyll-*c3* (chl-*c3*), peridinin (per), 19'-butanoyloxyfucoxanthin (19'-but), 19'- hexanoyloxyfucoxanthin (19'-hex), fucoxanthin (fuc), violaxanthin (viola), diadinoxanthin (diad), alloxanthin (allo), diatoxanthin (diat), zeaxanthin (zea), and β-carotene. Samples lacking any of the 17 pigments mentioned above were discarded from the analysis, leaving a total of 1397 samples that were used out of a total of 2950 samples.

2.5. Absorption coefficient of phytoplankton (a_{ph}).

Particulate absorption samples were collected on GF/F filters, and analysed as described in Stuart et al. (1998, 2000). Absorption by particulate matter ($a_p(\lambda)$) on wetted filters was measured between 400 and 750 nm relative to a blank saturated in filtered seawater, using a dual-beam Shimadzu UV-2101 PC scanning spectrophotometer with an integrating sphere (Stuart et al. 2000). Optical density measurements were divided by the geometrical path length (volume filtered divided by the clearance area of the filter) and multiplied by a factor of 2.3 to convert from decimal to natural logarithms. Detrital absorption, $a_d(\lambda)$, was estimated following the method of Kishino et al. (1985), as modified by Stuart et al. (1998). Pigments were extracted using 20 ml of a 6:4 (vol:vol) 90% acetone and dimethyl sulfoxide (DMSO), followed by 10 ml of filtered seawater to remove any residual solvents (Stuart et al. 1998), before the absorption by the extracted filters was measured. Since water-soluble phycobiliproteins are not readily extracted using this method, a correction was applied to avoid underestimation of the absorption by phytoplankton. The

189 detrital absorption spectrum was deconstructed into a series of Gaussian curves superimposed
190 onto an exponential curve at the wavelengths of the peak absorption by the non-extracted
191 pigments (420 and 666 nm for phaeopigments and 510, 550 and 590 nm for the biliproteins).
192 The Marquardt-Levenberg algorithm was used to determine the parameters which minimise
193 the sum of squares between the estimated and observed variables, giving a very good fit ($R^2 \sim$
194 0.99), before using the fitted exponential as the measure for detrital absorption. Absorption
195 coefficients were calculated by subtracting the optical density at 750 nm from all other
196 wavelengths, dividing by the geometrical path length (volume filtered divided by the
197 clearance area of the filter) and adjusting for path length amplification due to scattering by
198 the filter. Absorption by phytoplankton was calculated by subtracting $a_d(\lambda)$ from $a_p(\lambda)$. The
199 mean Chl *a*-specific absorption coefficient ($\bar{a}^*_{ph}$) was calculated by taking an average for all
200 values of a_{ph} between 400 and 700 nm and dividing by Chl *a*.

201 *2.6. Mean equivalent spherical diameter (MESD).*

202 The methods of Roy et al. (2011) were used to estimate MESD from measurements of a_{ph} and
203 pigment concentrations from HPLC. When approximated to homogeneous spheres, the
204 absorption characteristics of the cell are a function of the concentration of pigments and the
205 cell diameter. Due to the packaging effect, the absorption coefficient for a given
206 concentration of pigment in solution is greater than when it is contained within discrete
207 particles (Duysens 1956). Chl *a* is responsible for almost all the absorption at 676 nm. Since
208 the Chl *a* concentration in the samples is known, the degree of packaging can be calculated
209 by comparing the absorption by phytoplankton cells at 676 nm with the estimated absorption
210 at 676 nm from the same Chl *a* concentration using a hypothetical solution (Fig. 3). A lookup
211 table was then used to convert this measure of packaging into MESD. The table generates
212 values of ρ, which is the ratio between the light absorbed by a cell and the light incident on it,

for a given diameter *(d)* ranging from 0 to 500 μm, to enable approximate values for *d* to be calculated. See Roy et al. (2011) for further details.

2.7. Photosynthesis-Irradiance (PE) parameters

The protocol for the determination of *PE* parameters is described in Irwin (1990), Kyewelganga et al. (1997) and Bouman et al. (2005). Seawater samples were collected at the surface and at the chlorophyll maximum based on the *in vivo* fluorescence profile obtained from CTD casts. Thirty bottles were inoculated with 185 to 370 kBq (5 to 10 μCi) of ^{14}C-labelled bicarbonate and incubated for 2-3 hours. After the incubation, the seawater was filtered through 25 mm glass fibre filters (Whatman GF/F) at a vacuum pressure of < 200 mm Hg. The filters were exposed to concentrated HCl fumes to remove any inorganic carbon present, immersed in scintillation cocktail and the disintegration time per minute of ^{14}C was counted on a liquid scintillation counter. The *PE* parameters, P_m^B and α^B, were estimated by fitting the data to the model of Platt et al. (1980). The quantum yield of photosynthesis (φ_m) was calculated as:

$$\varphi_m = 0.0231\, \alpha^B / \bar{a}^*_{ph\,(400\text{-}700)} \qquad (3)$$

where $\bar{a}^*_{ph\,(400\text{-}700)}$ is the mean Chl *a*-specific absorption coefficient of phytoplankton, between 400 and 700 nm, and the constant 0.0231 in the numerator converts grams to moles and hours to seconds.

2.8. Statistical analysis

To examine physiological and ecological trends of phytoplankton communities, hierarchical cluster analysis was deployed using HPLC indicator pigment data and Ward's minimum variances clustering (Fig. 2). This is an agglomerative procedure where initially all points are considered singly, and merged in such a way to minimise the error sum of squares. The

number of clusters was determined as the point where adding extra clusters caused the error sum of squares to increase. The analysis was implemented in the statistical software R via the function "hclust" as part of the "stats" package 2.5.1 (http://cran.r-project.org). Effects of variations in total biomass were eliminated by using chlorophyll-normalised pigment concentrations. Data were plotted using package "ggplot2" version 0.8.9, and mapping package "Ocean data view" version 4. To run the cluster analysis it is necessary to have all pigments present in the sample, even at low concentrations, for the full matrix to be computed. Trends between phytoplankton community clusters, MESD, photosynthetic rates and environmental parameters were visualised as running averages and analysed using linear regressin using 'R'.

3. Results

3.1. Classification of phytoplankton communities.

Ward's minimum variance hierarchical clustering was used to classify the phytoplankton communities. The technique was applied to phytoplankton pigment concentrations normalised to Chl *a*, which characterised 8 principal clusters (Fig. 2) with distinctive pigment signatures (Fig. 3) size ranges (Fig. 4) *PE* parameters, and temperature and stratification indices (Fig. 5). Clusters 2 and 6 had the highest Chl *a* and fucoxanthin per unit Chl *a*, the largest mean cell size, P_m^B and the water masses associated with these clusters had the lowest mean temperature and stratification index. These clusters correspond with spring diatom populations (Fig. 3). Cluster 1 also had a relatively high fucoxanthin per unit Chl *a* *c*oncentration, though the mean equivalent spherical diameter (MESD) was lower than for cluster 2 and 6 (Fig. 4). This cluster represents a mixed assemblage of diatoms and prymnesiophytes. The phytoplankton community associated with Cluster 3 had a small mean cell size, with moderate to high zeaxanthin per unit Chl *a*, high α^B and low φ_m values, which

261 is indicative of picophytoplankton. Cluster 4 phytoplankton assemblage had high zeaxanthin
262 and Chl *b* per unit Chl *a* indicative of picophytoplankton, the lowest MESD and φ_m, high P_m^B
263 and the water mass associated with this cluster also had a high mean mixed-layer PAR.
264 Cluster 4 also had high concentrations of DVchl-*a* which is a key indicator of
265 *Prochlorococcus*. Cluster 5 occurred when PAR was low and is characterised by high
266 concentrations of Chl *b*, Chl *c*, 19'-hex, 19'-but, β-carotene per unit Chl *a*, which is indicative
267 of flagellates. Clusters 7 and 8 occurred during high stratification, and were characterised by
268 high concentrations of alloxanthin per unit Chl *a*, indicating the presence of cryptophytes or
269 photosynthetic ciliates such as *Mesodinium* spp.. Cluster 8 also had very high levels
270 concentrations of peridinim per unit Chl *a*.

271

272 *3.2.Seasonal succession in Phytoplankton communities and size.*

273 In early spring when the stratification index was low, clusters 6 and 2 were the most
274 abundant and are indicative of diatom blooms (Fig. 6). Both of these communities then
275 declined from Julian day 150 onwards when the stratification index increased and pico and
276 nanoeukaryote assemblages, represented by clusters 3 and 4, became dominant (Fig. 6).
277 During this period, cluster 1, the mixed assemblage of diatoms and prymnesiophytes, was
278 also present. By Julian day 250, clusters 3 and 4 decreased rapidly and cluster 1 also declined
279 and the dinoflagellate-dominated cluster 8 became more abundant. By Julian day 275 these
280 assemblages were replaced by flagellates dominated clusters 5 and 7, which peaked on Julian
281 day 300 and then declined by day 325, when the phytoplankton comprised a mixed
282 assemblage of clusters 1, 3, 4 and 8. By winter around Julian day 350, as the stratification
283 index became lower, clusters 3 and 4 decreased again, while cluster 5 reappeared (Fig. 6).

MESD was the highest in spring, decreased during the summer months, and then increased again in the autumn, though not to the same extent as in spring (Fig. 7c). Over all seasons, there was a significant positive correlation between MESD and total Chl *a* ($F_{1,1391}$ = 570, R^2 = 0.29, $p < 0.0001$; data not shown) and a significant negative correlation with the photosynthetic parameters (Table 3). There was also a significant negative correlation between MESD and temperature ($F_{1,1052}$ = 259.5, R^2 = 0.20, $p < 0.0001$; Fig 7a, Table 3) and the stratification index ($F_{1,1051}$ = 176, R^2 = 0.14, $p < 0.0001$; Fig 6b, Table 3).

3.3.Seasonal succession in photosynthetic rates.

During spring, clusters 3 (pico & nanoeukaryotes), 4 (pico & nanoeukaryotes) and 7 (flagellates) had the highest P_m^B (3, 3 and 3.5 mg C mg Chl a^{-1} hr^{-1}, respectively; Fig. 8a). During this period there seemed to be an anti-correlation with the dominant community since these clusters were in low abundance. In spring, clusters 1, 2 and 6 (all diatom dominated communities) were the most abundant but had the lowest P_m^B (<2, 2.5 and <1.5 mg C mg Chl a^{-1} hr^{-1}, respectively). By July (JD 210), clusters 4 and 7 continued to have the highest P_m^B values, which had increased to 5 and 4 mg C mg Chl a^{-1} hr^{-1}, respectively. Clusters 1 and 2 continued to have the lowest P_m^B values which had also increased slightly to 2.2 and 2.7 mg C mg Chl a^{-1} hr^{-1}, respectively. By September (JD270), clusters 4 and 7 reached their P_m^B maxima (6.6 and 5.9 mg C mg Chl a^{-1} hr^{-1}, respectively) and for clusters 5 (flagellates) and 8 (dinoflagellates), P_m^B values were >4.2 mg C mg Chl a^{-1} hr^{-1}. During this period, cluster 3 reached the lowest P_m^B values (<1.5 mg C mg Chl a^{-1} hr^{-1}). During the winter (JD360), cluster 5 had the highest values (>6 mg C mg Chl a^{-1} hr^{-1}) and cluster 1, which dominated the biomass, also reached its highest P_m^B (4 mg C mg Chl a^{-1} hr^{-1}; Fig. 8a).

For α^B in spring, all clusters exhibited similarly low values (0.01 – 0.03 mg C (mg Chl $a)^{-1}$ h^{-1}), with cluster 6 having slightly lower values and cluster 4 having higher values

compared to the overall mean (Fig. 8b). From spring to summer, there was an increase in α^B associated with each cluster which reached a peak in later summer. α^B then started to diverge in June (JD170) when cluster 5 had the lowest values and cluster 7, the highest. α^B continued to diverge in late summer (JD270) when clusters 1 & 7 were between 0.06 & 0.08 mg C (mg Chl *a*)$^{-1}$ h^{-1}, whereas clusters 3 & 8 only reached 0.02 mg C (mg Chl *a*)$^{-1}$ h^{-1} (Fig. 8b). Similarly, φ_m was low in spring and increased in summer when clusters 5 and 8 reached maximum values (Fig. 8c).

P_m^B and α^B were lower when MESD was high when clusters 1, 5 and 7 dominated, and were highest as MESD decreased when clusters 2, 3, 4 and 6 dominated (Fig. 7b, d). By contrast, φ_m exhibited the opposite trend and was higher when MESD was high and lower as MESD decreased (Fig. 7f). Similarly, P_m^B and α^B increased with increasing temperature and stratification index up to 20 °C and 0.1 stratification index when clusters 2, 3, 4 and 6 dominated (Fig. 9a, b). For all data, there were significant relationships between P_m^B and α^B and temperature, stratification index and PAR (Table 3). φ_m showed a slightly different pattern with a peak both in spring at ~2 °C, when the water column was still mixed, and in summer at 12 °C when the stratification index was 0.1 (Fig. 9g, h). Though there was a significant correlation between φ_m and PAR, there was no significant correlation between φ_m and temperature and stratification index (Fig. 9c, f, i, Table 3). .

4. Discussion

4.1. Phytoplankton community classification, size, succession and seasonality using bio-optical proxies.

Microscopy has been routinely used to characterise and enumerate phytoplankton since the 1950's (Utermöhl, 1958). Using this technique alone, very small phytoplankton (<3

μm) can be difficult to identify. Flow cytometry has therefore been deployed to identify small size phytoplankton (e.g. Moore et al., 2009). More recently, DNA and 18S rRNA probes have been used to quantify the abundance of picophytoplankton (e.g. Lie et al. 2014, Orsi et al. 2018). Signatures of phytoplankton pigments have also been used since the 1990's to elucidate the community structure of phytoplankton (e.g. Mackey et al. 1998). Automated HPLC allows for the rapid processing of pigments to determine phytoplankton groups, and a number of techniques have been developed to determine phytoplankton taxa from pigment signatures including CHEMTAX and pigment clusters (Mackey et al., 1998). In coastal waters there is generally good agreement between microscopy and HPLC pigment methods to derive phytoplankton community structure (Mackey et al. 1998). In Open Ocean oligotrophic waters, there was good agreement between the two techniques in the upper ocean, but disagreement between the two methods in deeper water samples has been reported due to depth-dependent changes in cellular pigment content and accessory pigment-to-chlorophyll ratios (Andersen et al. 1996). Brewin et al. (2014) compared HPLC and size fractionated filtration methods of deriving different phytoplankton groups and found that HPLC methods tended to under-estimate Chl *a* of picoplankton and over-estimate Chl *a* of nanophytoplankton compared to size filtration methods.

Lohrenz et al. (2003) used phytoplankton pigments to characterize size structure and community composition in relation to different water masses in Chesapeake Bay, USA and found that high salinity water was associated with haptophytes and dinoflagellates and low salinity water was associated with large diatoms. Similarly, Hill et al. (2005) used pigment ratios to identify successional trends in phytoplankton assemblages and found that large-sized fucoxanthin containing phytoplankton were associated with the higher primary production. None of these studies have used time series of phytoplankton pigments to elucidate climatological changes in community structure.

The successional trends that we observed are consistent with previous studies in the North Atlantic Ocean (Barlow et al., 1993, Lochte et al., 1993, Li 2002, Bouman et al., 2003). We found that MESD is large during spring, which is associated with high concentrations of fucoxanthin, predominantly from clusters 2 and 6, implying diatom dominance, when stratification is absent (Fig. 8), which has also been observed by Dandonneau & Niang (2007). Clusters 2 and 6 appear almost identical in terms of size, with the only visible difference being the higher concentration of β-carotene in cluster 6. β-carotene plays an important role in photo-protection (Llewellyn et al., 2005), but mean mixed-layer PAR was higher for cluster 2 compared to cluster 6. Chlorophyll-normalised β-carotene concentrations can be highly variable between different diatom species grown at the same irradiance (Dimier et al. 2007), which may partially explain this trend. There was a successional change from diatoms (Clusters 2 and 6) to a mixed assemblage of diatoms and prymnesiophytes (Cluster 1), followed by small eukaryotes with high concentrations of 19'-hex and 19'-but (Clusters 3 and 4) to nanoflagellates identified by Clusters 5 and 7 and finally dinoflagellates (Cluster 8). Cluster 1 had a lower MESD and very high chl-*a*-normalised concentrations of chl-*c1*, *c2* and *c3* unlike the other two fucoxanthin-dominated clusters (2 and 6), though there were no differences in the degree of stratification between these clusters. This decrease in MESD as the season progressed has also been observed in the seasonal succession of this and similar areas (Margalef 1978; Barlow et al., 1993; Lochte et al., 1993; Savidge et al., 1995; Irigoien et al., 2004; Llewellyn et al., 2005). The most difficult part of the annual succession to characterise using diagnostic pigments is the transition from diatoms to prymnesiophytes, which can both contain fucoxanthin. For Cluster 1, the association of fucoxanthin with chlorophylls-*c1, c2* and *c3* is more indicative of *Phaeocystis* than diatoms (Vaulot et al., 1994). In addition, there were 2 clusters identified with similar picophytoplankton populations. Cluster 3 is characterised by pico and nanoeukaryote pigment signatures. Cluster

382 4 has more cyanobacterial lineages as indicated by the presence of divinyl chlorophylls and
383 zeaxanthin. This shift in picophytoplankton community structure across oceanographic has
384 been reported more widely in global datasets (e.g. Bouman et al. 2011).

385

386 *4.2. Coupling between phytoplankton clusters, photosynthetic rates and environmental*
387 *parameters.*

388 An increasingly accepted paradigm is that marine phytoplankton communities are formed
389 from a background of smaller cells to which larger cells are added under conditions
390 favourable for growth, which increases Chl *a* and PP (Chisholm,1992; Li, 2002). In the
391 reverse direction, when the phytoplankton community becomes dominated by smaller cells,
392 Chl *a* and PP tend to decrease. The classic theory is that winter mixing followed by
393 stratification often results in high Chl *a*, photosynthetic rates and primary production
394 associated with microphytoplankton dominated by diatoms (Sverdrup, 1957). As
395 stratification intensifies, PAR and temperature also increase, but nutrients tend to decrease.
396 The phytoplankton community then becomes dominated by nano and picophytoplankton,
397 resulting in a decrease in Chl *a*, photosynthetic rates and primary production (Beardall et al.
398 2009). This has been shown in the North Atlantic, during the progression of the spring bloom
399 from diatoms to flagellates which is associated with lower maximum photochemical quantum
400 efficiency and higher absorption cross section of photosystem II and corresponds with a
401 decrease in cell size, a decrease in nutrients and increasing stratification (Moore et al. 2005).
402 Similarly in the upwelling regions off Baja California and the NW Iberian Peninsula, periods
403 of high stratification are associated with a decrease in photosynthetic rates and primary
404 production (Gomez-Ocampo et al., 2017; Tilstone et al., 2003).

A dichotomy exists around the community structure, cell size and the rate with which carbon is transferred through the ecosystem. Since smaller celled phytoplankton have a higher surface to volume ratio than larger cells, they have a greater ability to take up nutrients and absorb light, which could result in a higher photosynthetic efficiency (Cermeno et al., 2005). Under high nutrient concentrations and light however, large sized phytoplankton can attain higher Chl *a* normalized photosynthetic rates than smaller phytoplankton (Legendre et al. 1993; Tamigneaux et al. 1999), which suggests a higher physiological efficiency compared to smaller cells (Cermeno et al., 2005). There are an increasing number of studies however, that report an increase in photosynthetic rates and primary production during high stratification when nano and picophytoplankton dominate. In the North Pacific Subtropical Gyre for example, climate warming is associated with a shift in phytoplankton communities towards nano eukaryotes, and an increase in both Chl *a* and primary production even though dissolved silicate and phosphate have decreased (Karl et al. 2001). Similarly, in the Bay of Biscay, P_m^B is reported to be higher at the surface during summer when picophytoplankton dominate, which are positively correlated with stratification (Moran, 2007) and higher P_m^B was correlated with low diatom abundance (Moran and Sharek, 2015). By comparison, during cruises in spring and summer, PP decreased with increasing vertical stratification in the Mediterranean Sea (Estrada et al. 2014), but the relationship could be negative (during March), positive (during March and May) or non-existent (during September) depending on the time of year. Morán and Estrada (2005) reported that average P_m^B increased from winter to late-spring and summer, which was caused primarily by a change in the phytoplankton composition from relatively large to small cells. For all data, we found positive and significant correlations between P_m^B, α^B and temperature and stratification index indicating that in the NW Atlantic photosynthetic rates increase with temperature and water column stratification.

The variability in photosynthetic rates seems to be regional. For example, diatoms are reported to have the highest photosynthetic rates especially in upwelling zones due to replete light and nutrients (Babin, et al., 1996; Lorenzo, et al., 2005). In the open ocean, filamentous and colonial cyanobacteria, that have the ability to fix nitrogen, are also reported to have high photosynthetic rates (Li et al., 2011). Picophytoplankton is also reported to have high photosynthetic rates in some coastal and shelf seas (deMadariaga & Joint, 1994; Barnes, et al., 2014; Moran & Sharek, 2015; Platt et al., 1983).

In our analysis in the NW Shelf waters of the Atlantic, we found that pico and nanoeukaryotes had the highest photosynthetic rates and diatom dominated communities had the lowest rates. This is similar to the findings of Tilstone et al. (1999) in the NW Iberian Peninsula who showed that although microphytoplankton dominate the phytoplankton community, the highest and most variable photosynthetic rates are due to nanophytoplankton. In a temperate coastal ecosystem, Xie et al. (2015) showed that the succession from nanoeukaryotes (including *Phaeocystis* sp.) to dinoflagellates resulted in an increase in photosynthetic rates that is also associated with changes in temperature and nutrient regimes. By contrast, Mangoni et al. (2017) found in the Ross Sea that a diatom community dominated by *Pseudo-nitzschia* spp. had the highest photosynthetic rates whereas haptophytes had lower rates. Other studies have shown that small and subtle changes in phytoplankton community composition can result in high variability in photosynthetic rates. For example, Segura et al. (2013) found that in the Argentine Sea high variability in bio-optical and photosynthetic parameters due to adaptation to heterogeneous and highly dynamics environmental conditions. A community dominated by diatoms and coccal cells had the highest photosynthetic rates, whereas diatoms and *Emiliana huxlyei* had significantly lower rates.

All clusters except cluster 5 displayed positive relationships between φ_m and size (Fig 8a), indicating higher photosynthetic efficiency as size increases, possibly due to

455 compensation for a decrease in the efficiency of light-harvesting. It could also be the result of
456 larger values in MESD associated with high nutrient concentrations, which can increase φ_m
457 (Babin et al., 1996). This contrasts with the findings of Geider & Osborne (1986) who
458 observed no variation in φ_m in relation to changes in light regime or species. Finkel (2001)
459 and Ignatiades et al. (2002) also reported that φ_m decreases as cell size increases. We found a
460 negative relationship between φ_m and mean daily mixed-layer PAR for clusters 1, 4, 7 and 8
461 (Fig. 9b), which could be due to an increase in the concentration of photo-protective pigments
462 (Wilk-Woźniak et al., 2002, Babin et al., 1996). Since light absorbed by photo-protective
463 pigments is dissipated as heat, less energy is used for carbon fixation, and so theoretically φ_m
464 can decrease. For all data, both P_m^B, α^B and φ_m showed a significant negative correlation with
465 PAR (Table 3), indicating photo-acclimation to low light and photo-inhibition at high
466 irradiance. Negative relationships between mean daily PAR in the mixed layer and α^B were
467 specifically observed for clusters 1, 4, 7 and 8 (Fig. 9f). Clusters 2, 3, 5 and 6, however,
468 showed no such response. The mean values for α^B in these clusters are lower than those for
469 clusters 1, 4, 7 and 8 which did show a relationship between α^B and mean daily mixed-layer
470 PAR (Fig. 5, 9f). Given that the production of light-harvesting pigments is energetically
471 costly for phytoplankton (Raven 1984, Geider et al., 1996), cells that are subjected to higher
472 irradiances invest less energy in the synthesis of light-harvesting pigments, and α^B can
473 become lower. Alternatively the relationships may be the result of a reduction of functional
474 photosynthetic reaction centres due to photo-inhibition (Long et al., 1994), or nutrient stress
475 (Babin et al., 1996).

476 Using this cluster technique to characterise the phytoplankton community succession, we
477 were able to simultaneously characterise changes in size, environmental conditions and
478 photosynthetic parameters. As proof-of-concept, a robust relationship between MESD from flow
479 cytometry and absorption coefficients for the Scotian Shelf has been previously reported in Bouman

et al. (2003). P_m^B and α^B were highest when MESD was low, when nano and picophytoplankton dominated and when temperature (~20 °C) and stratification index (0.1) were high. These successional patterns in the dominant phytoplankton size-class and phenology support Margalef's (1978) mandala in terms of the relationship between turbulence and community structure. The study sheds new light on assemblages dominated by smaller cells, under warm, stratified conditions, having higher photosynthetic efficiencies, which has implications for the carbon flux on the NW Atlantic shelf.

Conclusion.

Using a dataset of HPLC phytoplankton pigments and phytoplankton absorption coefficients from the North West Atlantic, trends in phytoplankton distribution and succession were discerned. Cluster analysis on Chl *a* normalised accessory pigment concentrations revealed 8 distinct populations of phytoplankton with succession between the clusters dictated by seasonality and stratification. Fucoxanthin-dominated clusters, indicating the presence of diatoms, dominated in spring when turbulence was high. As stratification increased, MESD decreased and picophytoplankton increased, while in autumn, the strength of stratification decreased, and flagellates increased in importance. High values of MESD were associated with high Chl *a* concentrations, and a highly mixed water-column, in early spring, while smaller cells were observed during the summer, when the water-column was strongly stratified. For all except one cluster, a significant positive relationship between MESD and φ_m was observed, reflecting greater quantum efficiency as the efficiency of light absorption decreased due to self-shading. Negative relationships were also observed between α^B and mean mixed layer PAR during high stratification. Assemblages dominated by smaller cells during warm, stratified conditions in summer, had higher photosynthetic rates.

Acknowledgements

505 This work was supported by a NERC Studentship to A.R. (*Studentship No.* 0711560248004)
506 and is a contribution to the National Centre for Earth Observations Project of UK Natural
507 Environment Research Council, and to the ESA Project on Photosynthetic Parameters of
508 Phytoplankton from Space. G.H.T. was supported by UK Natural Environment Research
509 Council National Capability funding for the Atlantic Meridional Transect (AMT) to
510 Plymouth Marine Laboratory, which was also supported by near real time satellite service
511 from the National Earth Observation Data Archive and Analysis Service. We would like to
512 thank Jorn Bruggeman for his help in deriving the stratification indices. This is AMT
513 contribution number 329.

514

515 **References**

516 Alvain, S., Moulin, C., Dandonneau, Y., Loisel, H. 2008. Seasonal distribution and
517 succession of dominant phytoplankton groups in the global ocean: A satellite view.
518 Global Biogeochemical Cycles, 22, GB3001, doi:10.1029/2007GB003154

519 Álvarez, E., López-Urrutia, Á., Nogueira, E. Fraga, S., 2011. How to effectively sample the
520 plankton size spectrum? A case study using FlowCAM. Journal of Plankton Research,
521 33,1119-1133.

522 Álvarez, E., Moyano, M., Lopez-Urrutia, A., Nogueira, E., Scharek, R. 2014. Routine
523 determination of plankton community composition and size structure: a comparison
524 between FlowCAM and light microscopy J. Plankton Res. 36(1): 170–184.
525 doi:10.1093/plankt/fbt069Andersen, R.A., Bidigare, R.R., Keller, M.D., Latasa, M.
526 1996. A comparison of HPLC pigment signatures and electron microscopic

527 observations for oligotrophic waters of the North Atlantic and Pacific Oceans. Deep-
528 Sea Research II, 43(2-3): 517-537.

529 Anning, T., MacIntyre, H.L., Pratt, S.M., Sammes, P.J., Gibb, S., Geider, R.J., 2000.
530 Photoacclimation in the marine diatom Skeletonema costatum. Limnology and
531 Oceanography 45, 1807–1817.

532 Antonov, J.I., Seidov, D., Boyer, T.P., Locarnini, R.A., Mishonov, A.V., Garcia, H.E.,
533 Baranova, O.K., Zweng, M.M. Johnson, D.R., 2010. World Ocean Atlas *2009,*
534 *Volume 2: Salinity.* U.S. Government Printing Office.

535 Babin, M., Morel, A., Claustre, H., Bricaud, A., Kolber, Z. Falkowski, P.G., 1996. Nitrogen-
536 and irradiance-dependent variations of the maximum quantum yield of carbon fixation
537 in eutrophic, mesotrophic and oligotrophic marine systems. Deep Sea Research Part I:
538 Oceanographic Research Papers, 43, 1241-1272.

539 Barlow, R.G., Mantoura, R.F.C., Gough, M.A. Fileman, T.W., 1993. Pigment signatures of
540 the phytoplankton composition in the northeastern Atlantic during the 1990 spring
541 bloom. Deep Sea Research Part II: Topical Studies in Oceanography*,* 40, 459-477.

542 Barnes, M., Tilstone G.H., Smyth, T.J., Suggett, Kromkamp J, Astoreca R, Lancelot C. 2014.
543 Absorption based algorithm of primary production for total and size-fractionated
544 phytoplankton in coastal waters. Marine Ecology Progress Series 504: 73-89.

545 Beardall, J., Stojkovic, S., Larsen, S. 2009. Living in a high CO2 world: impacts of global
546 climate change on marine phytoplankton, Plant Ecology & Diversity, 2: 191-205.

547 Behrenfeld, M.J., Prasil, O., Babin, M., Bruyant, F., 2004. In search of a physiological basis
548 for covariations in light-limited and light-saturated photosynthesis. Journal of
549 Phycology 40, 4–25.

550 Booth, B.C., Lewin, J., Postel, J.R. 1993. Temporal variation in the structure of autotrophic
551 and heterotrophic communities in the subarctic Pacific. Progr. Oceanogr. 32(1–4), 57–
552 99.

553 Bouman, H., Platt, T., Sathyendranath, S., Stuart, V., 2005. Dependence of light-saturated
554 photosynthesis on temperature and community structure. Deep Sea Research Part I:
555 Oceanographic Research Papers, 52, 1284-1299.

556 Bouman, H., Platt, T., Sathyendranath, S., Li, W.K.W., Stuart, V., Fuentes-Yaco, C., Maass,
557 H., Horne, E.P.W., Ulloa, O., Lutz, V., Kyewalyanga, M., 2003. Temperature as
558 indicator of optical properties and community structure of marine phytoplankton:
559 Implications for remote-sensing. Marine Ecology Progress Series, 258, 19-30.

560 Bouman, H., Ulloa, O., Barlow, R., Li, W.K.W., Platt, T., Zwirglmaier, K., Scanlan, D.J.,
561 Sathyendranath, S., 2011. Water-column stratification governs the community
562 structure of subtropical marine phytoplankton. Environmental Microbiology Reports,
563 3, 473-482.

564 Brewin, R.J., Sathyendranath, S., Lange, P.K., Tilstone, G.H. 2014. Comparison of two
565 methods to derive size-structure of natural samples of phytoplankton. Deep-Sea
566 Research I, 85: 72-79.

567 Brewin, R.J.W., Tilstone, G.H., Jackson, T., Cain, T., Miller, P.I., Lange, P.K., Misra, A.,
568 Airs, R.L., 2017. Modelling size-fractionated primary production in the Atlantic
569 Ocean from remote sensing. Prog. Oceanogr. 158: 130-149.

570 Campbell, L., Olson, R.J., Sosik, H. M., Abraham, A., Henrichs, D.W., Hyatt, C.J., Buskey,
571 E.J. 2010. First harmful Dinophysis (Dinophyceae, Dinophysiales) bloom in the U.S.
572 is revealed by automated imaging flow cytometry. J. Phycol. 46: 66-75.

573 Cermeno, P., Estevez-Blanco, P., Maranon, E., Fernandez, E. 2005. Maximum photosynthetic
574 efficiency of size-fractionated phytoplankton assessed by 14C uptake and fast
575 repetition rate fluorometry. Limnol. Oceanogr. 50: 1438–1446.

576 Chauton, M., Tilstone, G.H., Legrand, C., Johnsen, G., Graneli, E., Sakshaug, E. 2004. The
577 effect of phytoplankton community structure and nutrient status on bio-optical and
578 photo-physiological changes during a phytoflagellate bloom. Journal of Plankton
579 Research, 26(3): 315-324.

580 Chisholm, S.W., 1992. Phytoplankton size. In: P.G. Falkowski, A.D. Woodhead, eds,
581 Primary productivity and biogeochemical cycles in the sea. Springer, pp. 213-237.

582 Dandonneau, Y. Niang, A., 2007. Assemblages of phytoplankton pigments along a shipping
583 line through the North Atlantic and tropical Pacific. Progress in Oceanography, 73,
584 127-144.

585 Claquin, P., Probert, I., Lefebvre, S., Veron, B., 2008. Effects of temperature on
586 photosynthetic parameters and TEP production in eight species of marine microalgae.
587 Aquatic Microbial Ecology 51, 1–11.

588 Clark, D., Widdicombe, C. E., Rees, A. P., Woodward, E. M. S. 2016. The significance of
589 nitrogen regeneration for new production within a filament of the Mauritanian
590 upwelling system. Biogeosciences, 13, 2873–2888.

591 Cloern, J.E. 1996. Phytoplankton bloom dynamics in coastal ecosystems. A review with
592 some general lessons from sustained investigation of San Francisco Bay, California.
593 Reviews of Geophysics 34, 127–168.

594 Daniels, C.J., Poulton, A. J., Esposito, M., Paulsen, M. L., Bellerby, R., St John, M., Martin,
595 A. P. 2015. Phytoplankton dynamics in contrasting early stage North Atlantic spring
596 blooms: composition, succession, and potential drivers. Biogeosciences, 12, 2395–
597 2409.

598 Detmer, A.,Bathmann,U.,1997.Distribution patterns of autotrophic pico and nanoplankton
599 and their relative contribution to algal biomass during spring in the Atlantic sector of
600 the Southern Ocean. Deep Sea Res. II44(1–2): 299–320.

601 deMadariaga, I., Joint, I.R., 1994. Photosynthesis and carbon metabolism by sizefractionated
602 phytoplankton in the southern North Sea in early summer. Cont. Shelf Res. 14, 95–
603 311.

604 Dimier, C., Corato, F., Tramontano, F,. Brunet, C., 2007. Photoprotection and xanthophyll-
605 cycle activity in three marine diatoms. Journal of Phycology, 43, 937-947.

606 Estrada, M., Latasa, M., Emelianov, M., Gutiérrez-Rodríguez , A., Fernández-Castro, B.,
607 Isern-Fontanet, J., Mouriño-Carballido, B., Salat, J., Vidal., M. 2014. Seasonal and
608 mesoscale variability of primary production in the deep winter-mixing region of the
609 NW Mediterranean. Deep-Sea Research I, 94: 45–61.

610 Finkel, Z.V., 2001. Light absorption and size scaling of light-limited metabolism in marine
611 diatoms. Limnology and Oceanography, 86-94.

612 Flynn, K.J., Clark, D. R., Mitra, A., Fabian, H., Hansen, P.J., Glibert, P.M., Wheeler, G.L.,
613 Stoecker, D.K., Blackford, J.C., Brownlee, C. 2015 Ocean acidification with
614 (de)eutrophication will alter future phytoplankton growth and succession. Proc. R.
615 Soc. B 282: 20142604. http://dx.doi.org/10.1098/rspb.2014.2604

616 Garmendia, M., Revilla, M., Zarauz, L. 2013. Testing the usefulness of a simple automatic
617 method for particles abundance and size determination to derive cost-effective
618 biological indicators in large monitoring networks. Hydrobiologia, 704: 231-252.

619 Geider, R., Osborne, B., 1986. Light absorption, photosynthesis and growth of *Nannochloris*
620 *atomus* in nutrient-saturated cultures. Marine Biology, 93, 351-360.

621 Geider, R.J., Macintyre, H.L., Kana, T.M., 1996. A dynamic model of photoadaptation in
622 phytoplankton. Limnology and Oceanography, 1-15.

623 Gomez-Ocampo, E., Durazo, R., Gaxiola-Castro, G. et al. 2017. Effects of the interannual
624 variability of water column stratification on phytoplankton production and biomass at
625 the north zone off Baja California. Ciencias Marinas, 43: 109-122.

626 Groben, R., John, U., Eller, G., Lange, M., Medlin, L., 2004. Using fluorescently-labelled
627 rRNA probes for hierarchical estimation of phytoplankton diversity - a mini review.
628 Nova Hedwigia, 79, 313-320.

629 Guidi, L., Stemmann, L., Jackson, G. A., Ibanez, F., Claustre, H., Legendre, L., Picheral, M.,
630 Gorsky, G. 2009. Effects of phytoplankton community on production, size and export
631 of large aggregates: A world-ocean analysis Limnol. Oceanogr., 54: 1951–1963.

632 Guidi, L., Chaffron, S., Bittner, L., Eveillard, D., Larhlimi, A., Roux, S., Darzi, Y., Audic, S.,
633 éo Berline, L., Brum, J.R., Coelho, L.P., Ignacio Espinoza, J. C., Malviya, S.,
634 Sunagawa, S., Dimier, C., Kandels-Lewis, S., Pichera, M., Poulain, J., Searson, S.,
635 Stemmann, L., Not, F., Hingamp, P., Speich, S., Follows, M., Karp-Boss, L., Boss, E.,
636 Ogata, H., Pesant, S., Weissenbach, J., Wincker, P., Acinas, S.G., Bork, P., de Vargas,
637 C., Iudicone, D., Sullivan, M.B**.,** Raes, J., Karsenti, E, Bowler, C., Gorsky1, G. 2016.
638 Plankton networks driving carbon export in the oligotrophic ocean. Nature, 532, 465-
639 470. doi:10.1038/nature16942

640 Head, E.J.H., Horne, E.P.W., 1993. Pigment transformation and vertical flux in an area of
641 convergence in the North Atlantic. Deep Sea Research Part II: Topical Studies in
642 Oceanography, 40, 329-346.

643 Hill, V., Cota, G., Stockwell, D. 2005. Spring and summer phytoplankton communities in the
644 Chukchi and Eastern Beaufort Seas. Deep-Sea Research II, 52(24-26): 3369-3385.

645 Ignatiades, L., Psarra, S., Zervakis, V., Pagou, K., Souvermezoglou, E., Assimakopoulou, G.,
646 Gotsis-Skretas, O., 2002. Phytoplankton size-based dynamics in the Aegean Sea
647 (Eastern Mediterranean). Journal of Marine Systems, 36, 11-28.

648 Irigoien, X., Flynn, K. J., Harris, R. P. 2005. Phytoplankton blooms: A 'loophole' in
649 microzooplankton grazing impact? J. Plankt. Res. 27: 313–321.

650 Irwin, A.J., Finkel, Z.V., Schofield, O.M.E., Falkowski, P.G., 2006. Scaling-up from nutrient
651 physiology to the size-structure of phytoplankton communities. Journal of Plankton
652 Research, 28, 459-471.

653 Jakobsen, H. H., Carstensen, J. 2011. FlowCAM: Sizing cells and understanding the impact
654 of size distributions on biovolume of planktonic community structure. Aquat Microb
655 Ecol., 65: 75–87, doi: 10.3354/ame01539

656 Jackett, D.R., Mcdougall, T.J., Feistel, R., Wright, D.W., Griffites, S.M., 2006. Algorithms
657 for density, potential temperature, conservative temperature, and the freezing
658 temperature of seawater. Journal of Atmospheric and Oceanic Technology, 23, 1709.

659 Jiang, L., Schofield, O.M., Falkowski, P.G., 2005. Adaptive evolution of phytoplankton cell
660 size. American naturalist, 496-505.

661 Karl, D.M., Bidigare, R.R., Letelier, R.M. 2001. Long-term changes in plankton community
662 structure and productivity in the North Pacific Subtropical Gyre: The domain shift
663 hypothesis. Deep-Sea Research II 48: 1449-1470.

664 Kiørboe, T., 1993. Turbulence, water column structure and phytoplankton cell size. Advances
665 in Marine Biology, 29, 1-72.

666 Kishino, M., Takahashi, M., Ichimura, S., 1985. Estimation of the spectral absorption
667 coefficients of phytoplankton in the sea. Bulletin of Marine Science, 37, 634-642.

668 Kyewalyanga, M.N., Platt, T., Sathyendranath, S. 1997. Estimation of the photosynthetic
669 action spectrum: implication for primary production models. Marine Ecology
670 Progress Series 146, 207–223.

671 Legendre, L., Gosselin, M., Hirche, H.J., Kattner, G., Rosenberg, G. 1993. Environmental
672 control and potential fate of size fractionated phytoplankton in the Greenland Sea
673 (758N). Marine Ecology Progress Series **98:** 297–313.

674 Li, W.K.W., Subba-Raio, D., Harrison, W.G., Smith, J.C., Cullen, J.J., Irwin, B., Platt,T.
675 1983.Autotrophic picoplankton in the tropical ocean. Science 219, 292–295.

676 Li, W.K.W., 2002. Macroecological patterns of phytoplankton in the northwestern North
677 Atlantic Ocean. Nature, 419, 154-157.

678 Li, B., Karl, D.M., Letelier, R.M., Church, M.J., 2011. Size-dependent photosynthetic
679 variability in the North Pacific Subtropical Gyre. Mar. Ecol. Prog. Ser. 440, 27–
680 40.Lie, A.A.Y., Liu, Z., Hu, S.K., Jones, A.C., Kim, D.Y., Countway, P.D., et al.
681 2014. Investigating microbial eukaryotic diversity from a global census: insights from
682 a comparison of pyrotag and full-length sequences of 18S rRNA genes. Appl.
683 Environ. Microbiol., 80: 4363–4373.

684 Llewellyn, C.A., Fishwick, J.R., Blackford, J.C., 2005. Phytoplankton community
685 assemblage in the English Channel: A comparison using chlorophyll a derived from
686 HPLC-CHEMTAX and carbon derived from microscopy cell counts. Journal of
687 Plankton Research, 27, 103-119.

688 Locarnini, R.A., Mishonov, A.V., Antonov, J.I., Boyer, T.P., Garcia, H.E., 2009. World
689 Ocean Atlas 2009, Volume 1, Temperature.

690 Lochte, K., Ducklow, H.W., Fasham, M.J.R., Stienen, C., 1993. Plankton succession and
691 carbon cycling at 47°N 20°W during the JGOFS North Atlantic Bloom Experiment.
692 Deep Sea Research Part II: Topical Studies in Oceanography, 40, 91-114.

693 Long, S., Humphries, S., Falkowski, P.G., 1994. Photoinhibition of photosynthesis in nature.
694 Annual review of plant biology, 45, 633-662.

695 Longhurst, A., Sathyendranath, S., Platt, T., Caverhill, C., 1995. An estimate of global
696 primary production in the ocean from satellite radiometer data. Journal of Plankton
697 Research, 17, 1245-1271.

698 Lohrenz, S.E. Carroll, C.L., Weidemann, A.D. 2003. Variations in phytoplankton pigments,
699 size structure and community composition related to wind forcing and water mass
700 properties on the North Carolina inner shelf. Continental Shelf Research, 23(14-15):
701 1447-1464.

702 Lorenzo LM, Arbones B, Tilstone GH, Figueiras F.G. 2005. Across-shelf variability of
703 phytoplankton composition, photosynthetic parameters and primary production in the
704 NW Iberian upwelling system. Journal of Marine Systems 54 (1-4): 157-173.Malone,
705 T.C. 1977. Light-saturated photosynthesis by phytoplankton size fractions in the New
706 York bight, USA. Mar. Biol. 42: 281–292.

707 Mackey, D.J., Higgins, H.W., Mackey, M.D., Holdsworth, D. 1998. Algal class abundances
708 in the western equatorial Pacific: Estimation from HPLC measurements of chloroplast
709 pigments using CHEMTAX. Deep-Sea Research I, 45(9): 1441-1468

710 Mangoni, O., Saggiomo, V., Bolinesi, F., Margiotta, F., Budillon, G., Cotroneo, Y., Misic,
711 C., Rivaro, P., Saggiomo, M. 2017. Phytoplankton blooms during austral summer in
712 the Ross Sea, Antarctica: Driving factors and trophic implications. PlosOne, 12(4):
713 e0176033. https://doi.org/10.1371/journal.pone.0176033

714 Margalef, R., 1978. Life-forms of phytoplankton as survival alternatives in an unstable
715 environment. Oceanologica acta, **134**, pp. 493-509.

716 Moore, C.M., Lucas, M.I., Sanders, R., Davidson, R. 2005. Basin-scale variability of
717 phytoplankton bio-optical characteristics in relation to bloom state and community
718 structure in the Northeast Atlantic. Deep-Sea Research I 52: 401-419.

719 Moore, C., Barnard, A., Fietzek, P., Lewis, M.R., Sosik, H.M., White, S., Zielinski, O., 2009.
720 Optical tools for ocean monitoring and research. Ocean Science, 5, 661-684.

721 Morán, X.A.G. 2007. Annual cycle of picophytoplankton photosynthesis and growth rates in
722 a temperate coastal ecosystem: a major contribution to carbon fluxes. Aquat Microb
723 Ecol. 49: 267–279.

724 Morán, X.A.G., Estrada, M. 2005. Winter pelagic photosynthesis in the NW Mediterranean,
725 Deep-Sea Research I, 52, 1806–1822.

726 Morán, X.A.G., Sharek, R., 2015. Photosynthetic parameters and primary production, with
727 focus on large phytoplankton, in a temperate mid-shelf ecosystem. Estuar. Coast.
728 Shelf Sci. 154, 255–263.

729 Morel, A., Bricaud, A. 1981. Theoretical Results Concerning Light-Absorption in a Discrete
730 Medium, and Application to Specific Absorption of Phytoplankton. Deep-Sea Res. I.
731 28, 1375-1393.

732 Munk, W.H., Riley, G.A. 1974. Absorption of nutrients by aquatic plants. J. Mar. Res.
733 11:215.

734 Nair, A., Sathyendranath, S., Platt, T., Morales, J., Stuart, V., Forget, M., Devred, E.,
735 Bouman, H., 2008. Remote sensing of phytoplankton functional types. Remote
736 Sensing of Environment, 112, 3366-3375.

737 Olson, R. J., Shalapyonok, A., Sosik, H. M. 2003. An automated submersible flow cytometer
738 for analysing pico and nanophytoplankton: FlowCytobot. Deep-Sea Research I 50:
739 301–315.

740 Orsi W.D., Wilken S., del Campo, J., Heger, T., James, E., Richards, T. A., Keeling, R. J.,
741 Worden, A.Z., Santoro, A.E. 2018. Identifying protist consumers of photosynthetic
742 picoeukaryotes in the surface ocean using stable isotope probing. Environ. Microbio.,
743 20(2), 815–827. doi:10.1111/1462-2920.14018.

744 Pahlow, M., Riebesell, U., Wolf-Gladrow, D.A. 1997. Impact of cell shape and chain
745 formation on nutrient acquisition by marine diatoms. Limnol. Oceanogr., 42, 1660-
746 1672.

747 Platt, T., Gallegos, C., Harrison, W., 1980. Photoinhibition of photosynthesis in natural
748 assemblages of marine phytoplankton. Journal of Marine Research, 38.

749 Platt, T., Rao, D.V.S., Irwin, B., 1983. Photosynthesis of picoplankton in the oligotrophic
750 ocean. Nature 301, 702–704.

751 Platt, T., Fuentes-Yaco, C K.T.F., 2003. Marine ecology: spring algal bloom and larval fish
752 survival. Nature, 423, 398-399.

753 R Core Development Team 2009. R: A language and environment for statistical computing.
754 R foundation for Statistical Computing, Vienna, Austria. ISBN 3-900051-07-0, URL
755 http://www.R-project.org

756 Raven, J.A., 1984. Physiological correlates of the morphology of early vascular plants.
757 Botanical Journal of the Linnean Society, 88, 105-126.

Raven, J.A., 1998. The twelfth Tansley lecture: Small is beautiful: The picophytoplankton. Functional ecology, 12, 503-513. Richardson, T.L., Jackson, G.A. 2007. Small Phytoplankton and Carbon Export from the Surface Ocean. Science, 315, 838-840. DOI: 10.1126/science.1133471

Riegman, R., Kraay, G.W. 2001. Phytoplankton community structure derived from HPLC analysis of pigments in the Faroe-Shetland Channel during summer 1999: the distribution of taxonomic groups in relation to physical/chemical conditions in the photic zone. Journal of Plankton Research, 23: 191-205.

Robinson, A., Bouman, H.A., Tilstone, G.H., Sathyendranath, S. (2018). Size class dependent relationships between temperature and phytoplankton photosynthesis-irradiance parameters in the Atlantic Ocean. Frontiers in Marine Science, 4:435, doi: 10.3389/fmars.2017.00435

Roy, S., Sathyendranath, S., Platt, T., 2011. Retrieval of phytoplankton size from bio-optical measurements: theory and applications. Journal of The Royal Society Interface, 8, 650-660.

Sathyendranath, S., Stuart, V., Platt, T., Bouman, H., Ulloa, O., Maass, H., 2005. Remote sensing of ocean colour: Towards algorithms for retrieval of pigment composition. Indian Journal of Marine Sciences, 34, 333-340.

Savidge, G., Boyd, P., Pomroy, A., Harbour, D., Joint, I., 1995. Phytoplankton production and biomass estimates in the northeast Atlantic Ocean, May-June 1990. Deep-Sea Research Part I: Oceanographic Research Papers, 42, 599-617.

779 Segura V, Lutz VA, Dogliotti A, Silva RI, Negri RM, Akselman R, Benavides H (2013)
780 Phytoplankton types and primary production in the Argentine Sea. Mar Ecol Prog Ser
781 491:15-31.

782 Sieracki, M.E., Verity, P.G., Stoecker, D.K., 1993. Plankton community response to
783 sequential silicate and nitrate depletion during the 1989 North Atlantic spring bloom.
784 Deep-Sea Research Part II, 40, 213-225.

785 Stuart, V., Sathyendranath, S., Head, E.J.H., Platt, T., Irwin, B., Maass, H., 2000. Bio-optical
786 characteristics of diatom and prymnesiophyte populations in the Labrador Sea. Marine
787 Ecology Progress Series, 201, 91-106.

788 Stuart, V., Sathyendranath, S., Platt, T., Maass, H., Irwin, B.D., 1998. Pigments and species
789 composition of natural phytoplankton populations: Effect on the absorption spectra.
790 Journal of Plankton Research, 20, 187-217.

791 Sverdrup, H. U. 1957. On conditions for the vernal blooming of phytoplankton. Journal du
792 Conseil International pour l'Exploration de la Mer, 18, 287–295.

793 Tamigneaux, E., Legendre, L., Klein, B., Mingelbier, M. 1999. Seasonal dynamics and
794 potential fate of size-fractionated phytoplankton in a temperate nearshore environment
795 (Western Gulf of St. Lawrence, Canada). Estuarine Coastal Shelf Science 48: 253–
796 269.

797 Tilstone, G.H., Figueiras, F.G., Fermín, E.G., Arbones, B. 1999. The significance of nano-
798 phytoplankton photosynthesis and primary productivity in a coastal upwelling
799 ecosystem (Ría de Vigo, NW Spain). Marine Ecology Progress Series 183: 13-27.

800 Tilstone, G.H., Lorenzo, L.M., Arbones, B., Figueiras, F.G. 2003. Photosynthesis primary
801 production and phytoplankton growth rates different hydrographic conditions at the
802 NW Iberian upwelling margin. Marine Ecology Progress Series, 252: 89-104.

803 Waite, A.M., Safi, K.A., Hall, J.A., Nodder, S.D., 2000. Limnol. Oceanogr. 45, 87.
804 Uitz, J., Huot, Y., Bruyant, F., Babin, M., Claustre, H., Claustre, H., 2008. Relating
805 Phytoplankton Photophysiological Properties to Community Structure on Large
806 Scales. Limnology and Oceanography, 53, 614-630.

807 Utermöhl, H., 1958. Perfeccionamento del método cuantitativo del fitoplancton. Comum.
808 Assoc. Int. Limnol. Teor. Apl. 9,1–89.

809 Vaulot, D., Birrien, J., Marie, D., Casotti, R., Veldhuis, M.J.W., Kraay, G.W., Chrétiennot-
810 Dinet, M., 1994. Morphology, ploidy, pigment composition, and genome size of
811 cultured strains of *Phaeocystis* (Prymnesiophyceae). Journal of Phycology, 30, 1022-
812 1035.

813 Wassmann, P., Ratkova, T., Reigstad, M., 2005. The contribution of single and colonial cells
814 of *Phaeocystis pouchetii* to spring and summer blooms in the north-eastern North
815 Atlantic. Harmful Algae, 4, 823-840.

816 Wickham, H., 2009. ggplot2: Elegant Graphics for Data Analysis. 2nd edn. Springer
817 Publishing Company, Incorporated.

818 Wilk-Woźniak, E., Pociecha, A., Bucka, H., 2002. Phytoplankton-zooplankton interactions,
819 size relations and adaptive responses. A short review. Ecohydrology and
820 Hydrobiology, 1, 511-517.

821 Xie Y., Tilstone G.H., Widdicombe, C., Woodward, E.M.S., Harris, C., Barnes, M.K. 2015.
822 Effects of increases in temperature and nutrients on phytoplankton community
823 structure and photosynthesis in the Western English Channel. *Marine Ecology*
824 *Progress Series* 519: 61-73. doi: 10.3354/meps11101

825

826 **Figure Legends.**

827 **Fig. 1.** Station locations in the North Atlantic used for cluster analysis of HPLC
828 phytoplankton pigment data.

829 **Fig. 2.** Results of Ward's hierarchical cluster analysis using chlorophyll-normalised HPLC
830 pigment concentrations. (a) Descent curve showing clear elbow at 8 clusters. (b) Dendrogram
831 showing Euclidian distances between samples, with cluster numbers.

832 **Fig. 3.** Boxplots showing (a) Percentage of total Chl-*a* which is divinyl, (b) Chl-*a* normalised
833 chl-*b*, (c) Chl-*a* normalised combined chl-*c1* and chl-*c2*, (d) Chl-*a* normalised β-carotene, (e)
834 Chl-*a* normalised chl-*c3*, (f) Chl-*a* normalised fucoxanthin, (g) Chl-*a* normalised peridinin,
835 (h) Chl-*a* normalised alloxanthin, (i) Chl-*a* normalised 19'-butanoyloxyfucoxanthin, (j) Chl-*a*
836 normalised 19'-hexanoyloxyfucoxanthin, (k) Chl-*a* normalised zeaxanthin.

837 **Fig. 4**. Density plots of the size distributions of different phytoplankton populations from
838 hierarchical cluster analysis on chlorophyll normalised HPLC pigment concentrations. Lines
839 coloured according to cluster. Cluster 1: red, 2: green, 3: dark blue, 4: light blue, 5: purple, 6:
840 yellow, 7: grey, 8: pink. Size structure estimated using absorption at 676nm.

841 **Fig. 5.** Boxplots showing photosynthetic parameters and chlorophyll normalised HPLC
842 pigment concentrations for the different clusters. (a.) Total chlorophyll-*a* (μg/l), (b.)
843 Temperature (^{o}C), (c.) Photosynthetically active radiation (E m^{-2} d^{-1}), (d.) φ_m (E m^{-2} d^{-1}), (e.)
844 P_m^B (mgC (mg chl-*a*)$^{-1}$ h^{-1}), (f.) α^B (mg C (mg chl-*a*)$^{-1}$ h^{-1} μmol quanta m^{-2} s^{-1})$^{-1}$, (g.) Mean
845 equivalent spherical diameter from absorption (μm), (h.) Stratification index, defined as the
846 difference between samples temperature and climatological prediction for the temperature at
847 100m / offset in depth (^{o}C m^{-1}), (i.) proportion of divinyl Chl *a*.

Fig. 6. (a) Proportion of samples in each cluster with respect to Julian day in North West Atlantic Shelf Province as defined by Longhurst et al. (1995). Clusters assigned using hierarchical cluster analysis on Chl-*a* normalised HPLC pigments. (b) Proportion of samples in each cluster with respect to the degree of stratification in the North West Atlantic Shelves Stratification index is defined as the difference between sample temperature and climatological prediction for the temperature at 100 m divided by the offset in depth.

Fig. 7. Relationship between mean equivalent spherical diameter and environmental and biological variables; (a.) temperature, (b.) P_m^B, (c.) Julian Day, (d.) α^B, (e.) stratification index, (f.) φ_m. Points are coloured according to phytoplankton cluster as assigned using chlorophyll normalised hierarchical cluster analysis. Cluster 1: red, 2: green, 3: dark blue, 4: light blue, 5: purple, 6: yellow, 7: grey, 8: pink. Black line is the running average of all points.

Fig. 8. Relationship between (a.) maximum photosynthetic rate (P_m^B; mg C mg Chl a^{-1} hr^{-1}), (b.) light limited slope of photosynthesis (α^B (mg C (mg chl-*a*)$^{-1}$ h^{-1} µmol quanta m^{-2} s^{-1})$^{-1}$) (c.) maximum quantum yield (φ_m (E m^{-2} d^{-1})) for each cluster and time of the year (Julian Day). Coloured lines are the running average for each cluster.

Fig. 9. Relationship between P_m^B (mg C mg Chl a^{-1} hr^{-1}) and (a.) temperature, (b.) stratification index, (c.) mean PAR in the mixed layer (E m^{-2} d^{-1}); α^B (mg C mg chl-*a*)$^{-1}$ h^{-1} µmol quant m^{-2} s^{-1})$^{-1}$ and (d.) temperature, (e.) stratification index, (f.) mean PAR in the mixed layer (E m^{-2} d^{-1}); and φ_m (mol C (mol quanta)$^{-1}$), (g.) temperature, (h.) stratification index, (i.) mean PAR in the mixed layer (E m^{-2} d^{-1}). Points are coloured according to hierarchical cluster analysis on chlorophyll normalised HPLC pigments. Black line is the running average of all points.

Table 1. Summary of key cluster properties, showing sample temperature, depth, day of year, total HPLC chl-*a, PE* parameters, quantum yield (φ_m), mean-specific absorption between 350

872 and 700 nm ($\bar{a}_{ph}^{*}$). Mean phytoplankton MESD was estimated using phytoplankton absorption
873 coefficients (Roy et al. 2011).

874 **Table 2**. Summary of pigments present in the different clusters and ecological implications.

875 **Table 3**. Statistical relationships between environmental variables and (A.) mean equivalent
876 spherical diameter, (b.) photosynthetic rates using linear regression. R^2 is the coefficient of
877 variation, F is the mean square to mean square error ratio, df denotes the degrees of freedom
878 and P is the critical significance value.

879

880

Table 1. Summary of key cluster properties, showing sample temperature, depth, day of year, total HPLC chl-*a, PE* parameters, quantum yield (φ_m), mean-specific absorption between 350 and 700 nm ($\bar{a}^*_{ph}$). Mean phytoplankton ESD was estimated using absorption (Roy *et al.* 2011).

		Pigment-based clustering								
	Cluster	**1**	**2**	**3**	**4**	**5**	**6**	**7**	**8**	**All**
	n	187	311	228	158	77	83	188	165	1397
Temp (°C)	Min	-0.9	-1.6	-1.2	-1.5	3.2	-1	1	-0.4	-1.6
	Mean	4.6	3.6	11.6	11.6	9.6	3.2	9.8	7.8	7.9
	Max	19.3	16.1	23.2	26.3	24.2	10.1	19.4	15.7	26.3
	SD	3.6	3.1	5.3	8.4	5.9	3	3.9	3.3	6.0
Depth (m)	Min	0	1	0	1	1	0	1	1	0
	Mean	18.6	13.6	14	21.5	7.8	13.5	8	7.7	13.5
	Max	125	80	130	170	50	51	45	50	170
	SD	19.1	15.4	17.7	29.3	11.6	14.3	10.6	11.3	17.9
Julian day	Min	98	65	84	79	83	65	98	98	65
	Mean	200	133	241.4	173.6	246	111.4	248.7	230.4	197
	Max	355	356	340	340	355	184	353	351	356
	SD	88.4	55.7	62.4	85.6	79.0	27.5	78.0	87.0	87.1
Total Chl-*a* (µg/l)	Min	0.095	0.043	0.073	0.014	0.104	0.35	0.14	0.20	0.014
	Mean	1.24	2.30	0.55	0.36	1.17	4.74	0.94	0.98	1.40
	Max	6.74	13.85	2.42	2.81	7.55	28.0	3.20	4.47	27.97
	SD	1.20	2.63	0.42	0.39	1.29	4.15	0.53	0.63	2.02
P_m^B	Min	0.41	0.42	0.79	0.43	0.74	0.33	0.99	0.57	0.33
	Mean	2.36	2.46	3.3	3.95	3.53	1.87	4.66	3.08	3.10
	Max	6.95	19.73	12.7	12.54	7.69	4.55	9.36	7.46	19.73
	SD	1.29	1.86	2	2.51	2.31	1.02	1.99	1.36	2.02
α^B	Min	0.0043	0.0039	0.0089	0.0029	0.0093	0.0043	0.012	0.0064	0.0029
	Mean	0.034	0.024	0.041	0.034	0.042	0.016	0.047	0.028	0.034
	Max	0.116	0.181	0.088	0.120	0.099	0.040	0.117	0.058	0.181
	SD	0.023	0.021	0.020	0.024	0.029	0.0071	0.022	0.011	0.022
φ_m	Min	0.0050	0.0054	0.0069	0.00036	0.0094	0.0054	0.0073	0.0065	0.00036
	Mean	0.037	0.036	0.022	0.022	0.039	0.030	0.043	0.025	0.034
	Max	0.146	0.291	0.086	0.082	0.098	0.086	0.095	0.123	0.291
	SD	0.027	0.029	0.020	0.021	0.029	0.018	0.023	0.019	0.025
Mean specific absorption (400-700 nm)	Min	0.0085	0.0051	0.014	0.019	0.010	0.0044	0.011	0.0085	0.0043
	Mean	0.027	0.019	0.034	0.066	0.026	0.014	0.026	0.031	0.030
	Max	0.095	0.076	0.099	0.505	0.065	0.054	0.066	0.085	0.505
	SD	0.014	0.011	0.014	0.064	0.0084	0.0081	0.0082	0.013	0.028
Size from absorption (µm)	Min	0.1	0.1	0.1	0.1	0.1	0.1	0.1	0.1	0.1

Table 2: Summary of pigments present in different clusters and the ecological implications. For the proportion of total accessory pigments: Red = chl-*b*, Green = chl-*c*1*c*2, Dark blue = chl-*c*3, Light blue = fuc, Magenta = per, Yellow = allo, Grey = 19'-but, Black = 19'-hex, Orange = β-carotene, Pink = zea

Proportions of pigments in sample	Cluster number	Important pigments	Ecological implications
	**1**	Fuc, chl-*c*1, *c*2, *c*3	Small diatoms / *Phaeocystis*. Late spring / early summer
	**2**	Fuc, chl-*c*1, *c*2	Large diatoms. Spring, very large MESD
	**3**	Chl-*b*, chl-*c*3, 19'-hex, 19'-but	Picoeukaryotes. Summer, very highly stratified. Some small dino-flagellates, no *Prochlorococcus*
	**4**	Chl-*b*, divinyl chl-*a*, zea. Some 19'-hex, yet 19'-but absent	Picoeukaryotes and prokaryotes. Only cluster with significant pro-portion of *Prochlorococcus*. Summer, stratified
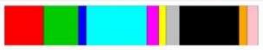	**5**	Chl-*b*, 19'-hex, 19'-but, β-carotene, some allo	Nanophytoplankton including chrysophytes. Late summer / early autumn. Less stratified than cluster 7.
	**6**	Fuc, chl-*c*1, *c*2, β-carotene	Large diatoms, similar to cluster 2, very large MESD. Early spring.
	**7**	Chl-*b*, allo, 19'-hex, 19'-but	Nanophytoplankton, more stratified than cluster 5. Very high φ_m and P_m^B.
	**8**	Per, allo	Present throughout the season. Dinoflagellate dominated. Large difference in MESD according to method.

Table 3. Statistical relationships between environmental variables and (A.) mean equivalent spherical diameter, (b.) photosynthetic rates using linear regression. R^2 is the coefficient of variation, F is the mean square to mean square error ratio, df denotes the degrees of freedom and P is the critical significance value.

A.	**Slope**	**Intercept**	**R^2**	**F**	**df**	**P**
MESD v temperature	-0.91	25	0.20	260	1,1052	<0.0001
MESD v P_m^B	-1.186	21.1	0.03978	31.03	724	<0.0001
MESD v α^B	-90.1	20.5	0.02796	21.86	724	<0.0001
MESD v φ_m	210.6	8.0038	0.2085	188.9	712	<0.0001
MESD v stratification	-95	20	0.14	176	1,1052	<0.0001
B.						
P_m^B v temperature	0.191	1.75	0.3031	315.9	723	<0.0001
α^B v temperature	0.00121	0.0248	0.0972	78.99	723	<0.0001
φ_m v temperature	-0.000403	0.048	0.006993	6.014	711	0.014
P_m^B v stratification	20.84	2.684	0.26	255.6	723	<0.0001
α^B v stratification	0.193	0.0295	0.181	161.3	723	<0.0001
φ_m v stratification	-0.0255	0.0457	0.001039	1.74	711	0.1875
P_m^B v PAR	-0.0373	3.959	0.0153	6.76	370	0.00967
α^B v PAR	-0.000597	0.042	0.041	17.04	370	<0.0001
φ_m v PAR	-0.000936	0.0475	0.07392	30.45	368	<0.0001

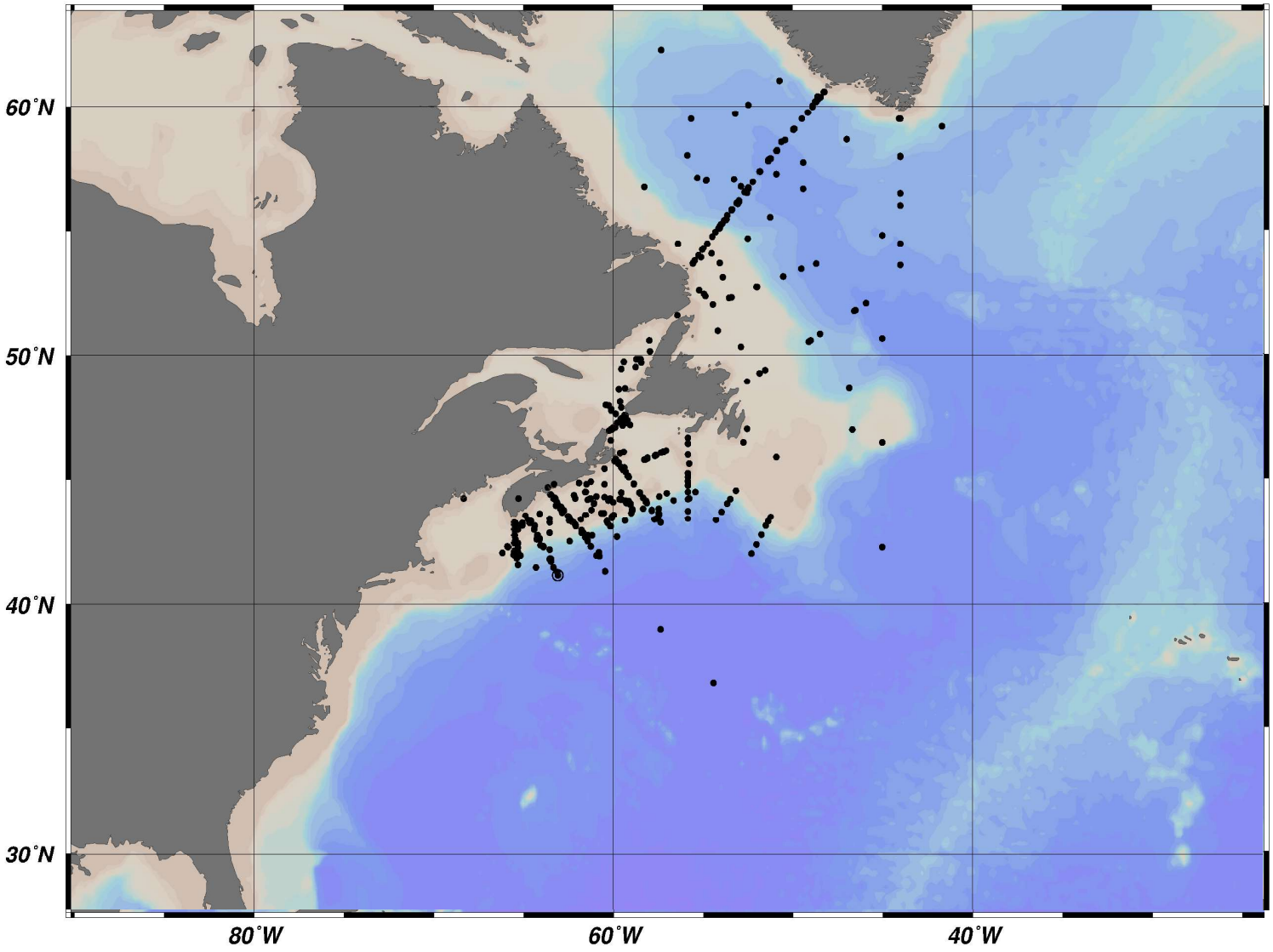
60˚N
50˚N
40˚N
30˚N
80˚W
60˚W
40˚W

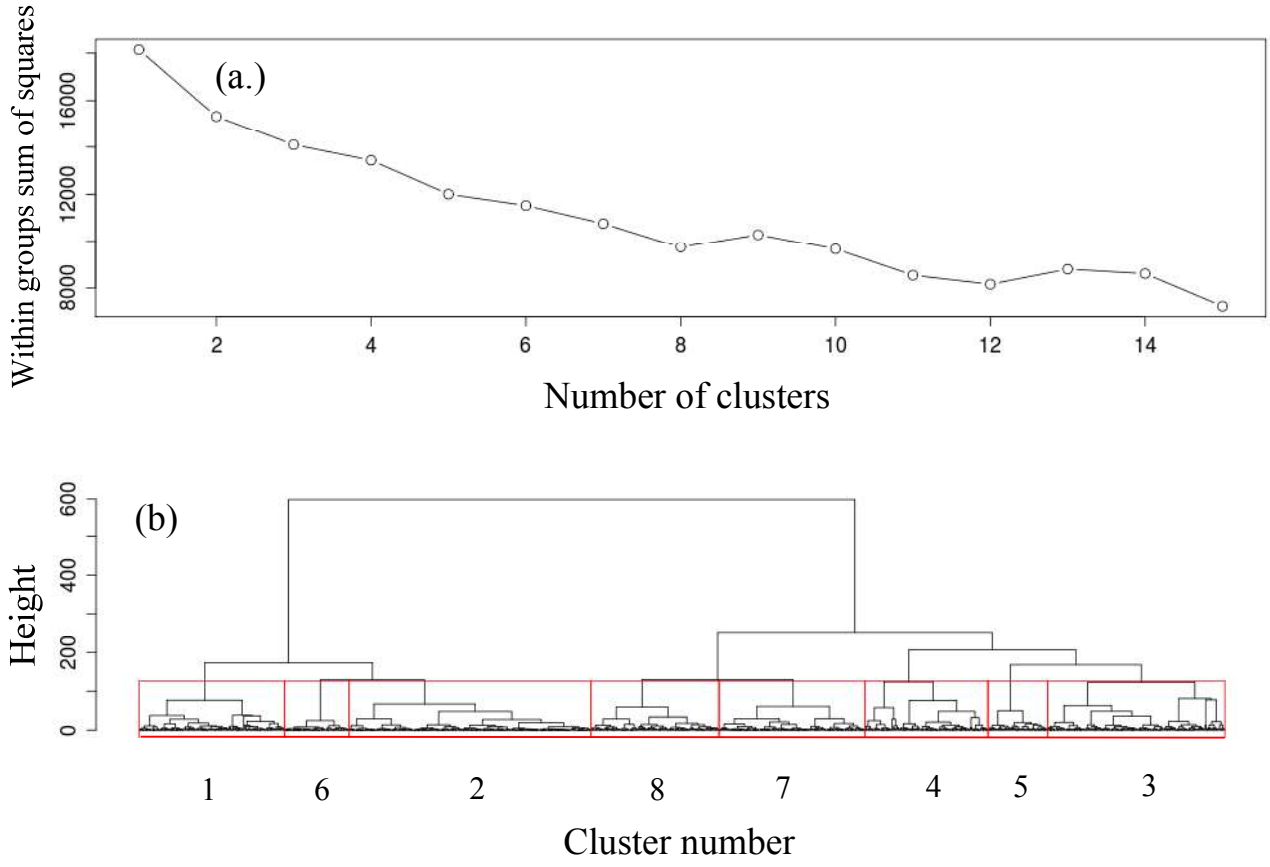

Figure 2. Results of Ward's hierarchical cluster analysis using chlorophyll-normalised HPLC pigment concentrations. (a) Descent curve showing clear elbow at 8 clusters. (b) Dendrogram showing Euclidian distances between samples, with cluster numbers.

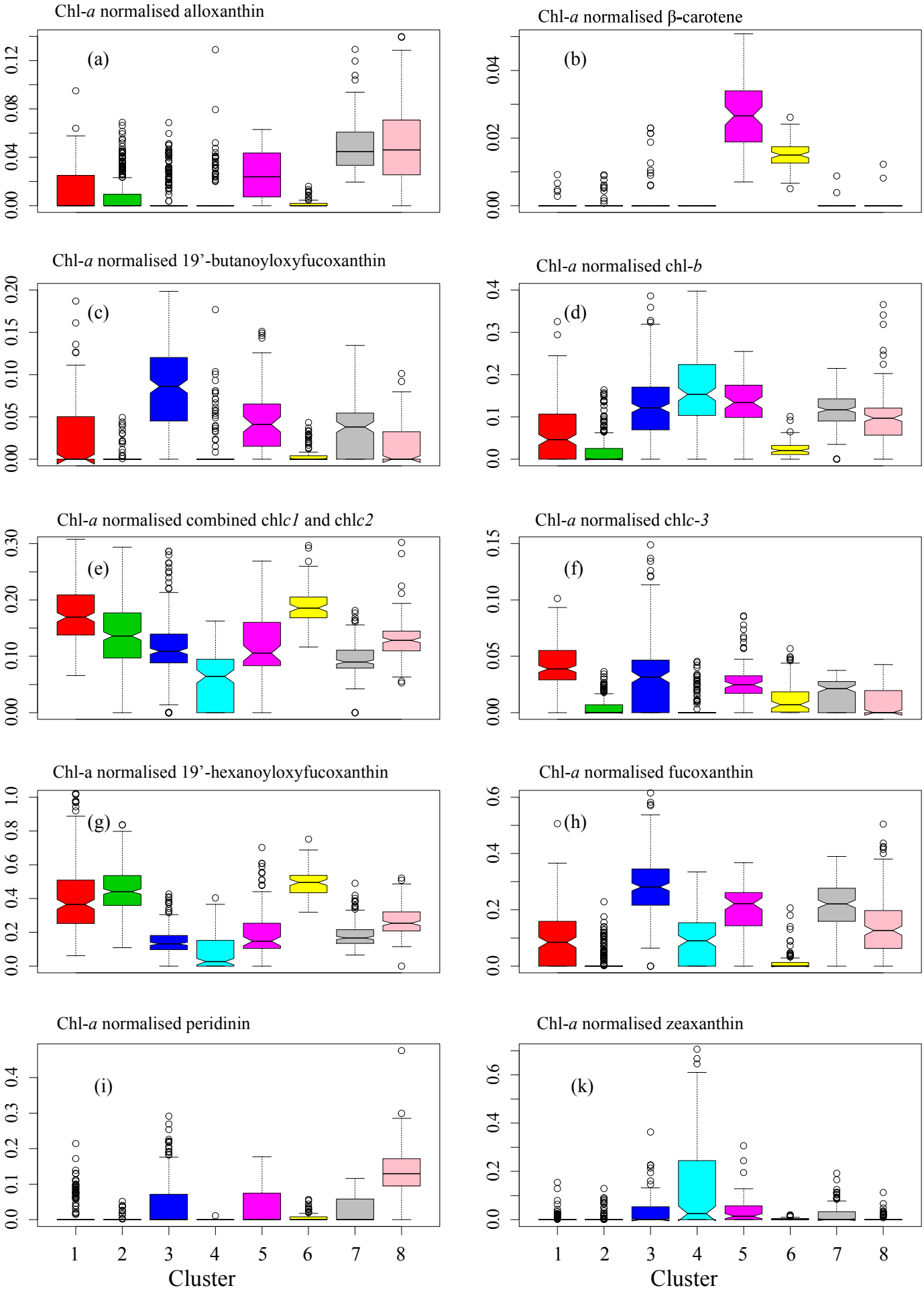
Chl-a normalised alloxanthin
(a)
0.00
0.04
0.08
0.12
Chl-a normalised β-carotene
(b)
0.00
0.02
0.04
Chl-a normalised 19'-butanoyloxyfucoxanthin
(c)
0.00
0.05
0.10
0.15
0.20
Chl-a normalised chl-b
(d)
0.0
0.1
0.2
0.3
0.4
Chl-a normalised combined chlc1 and chlc2
(e)
0.00
0.10
0.20
0.30
Chl-a normalised chlc-3
(f)
0.00
0.05
0.10
0.15
Chl-a normalised 19'-hexanoyloxyfucoxanthin
(g)
0.0
0.2
0.4
0.6
0.8
1.0
Chl-a normalised fucoxanthin
(h)
0.0
0.2
0.4
0.6
Chl-a normalised peridinin
(i)
0.0
0.1
0.2
0.3
0.4
Chl-a normalised zeaxanthin
(k)
0.0
0.2
0.4
0.6
1
2
3
4
5
6
7
8
Cluster
1
2
3
4
5
6
7
8
Cluster

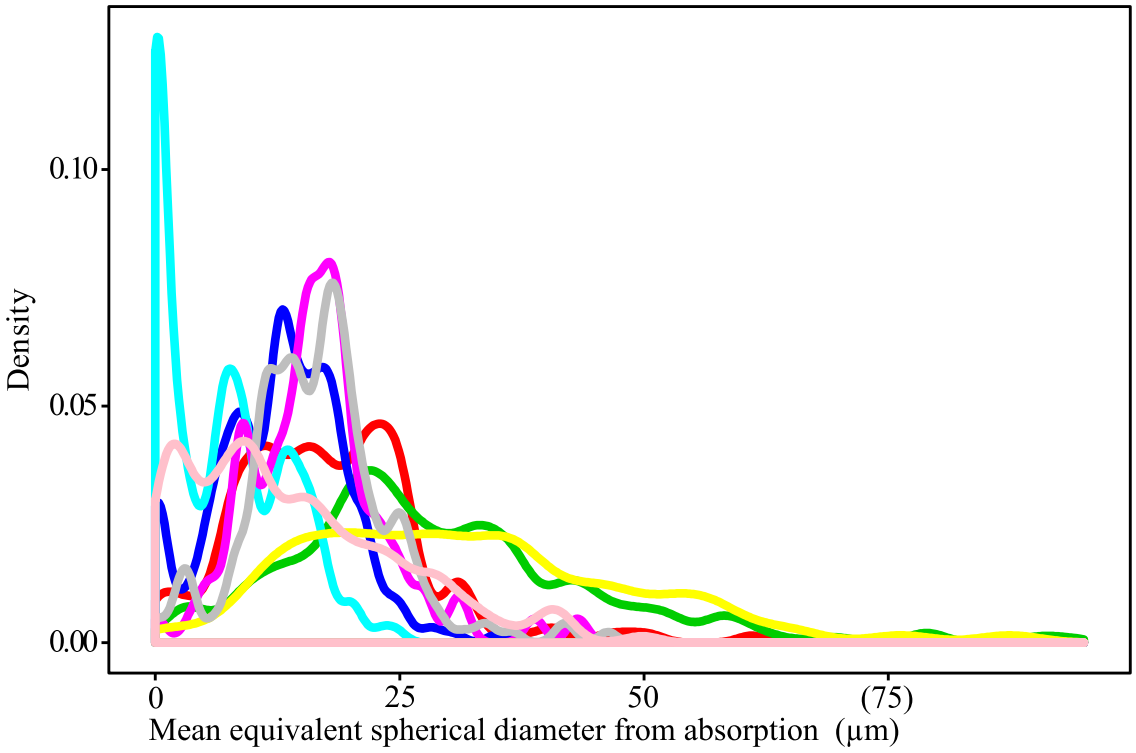
Density
0.10
0.05
0.00
0
25
50
(75)
Mean equivalent spherical diameter from absorption (µm)

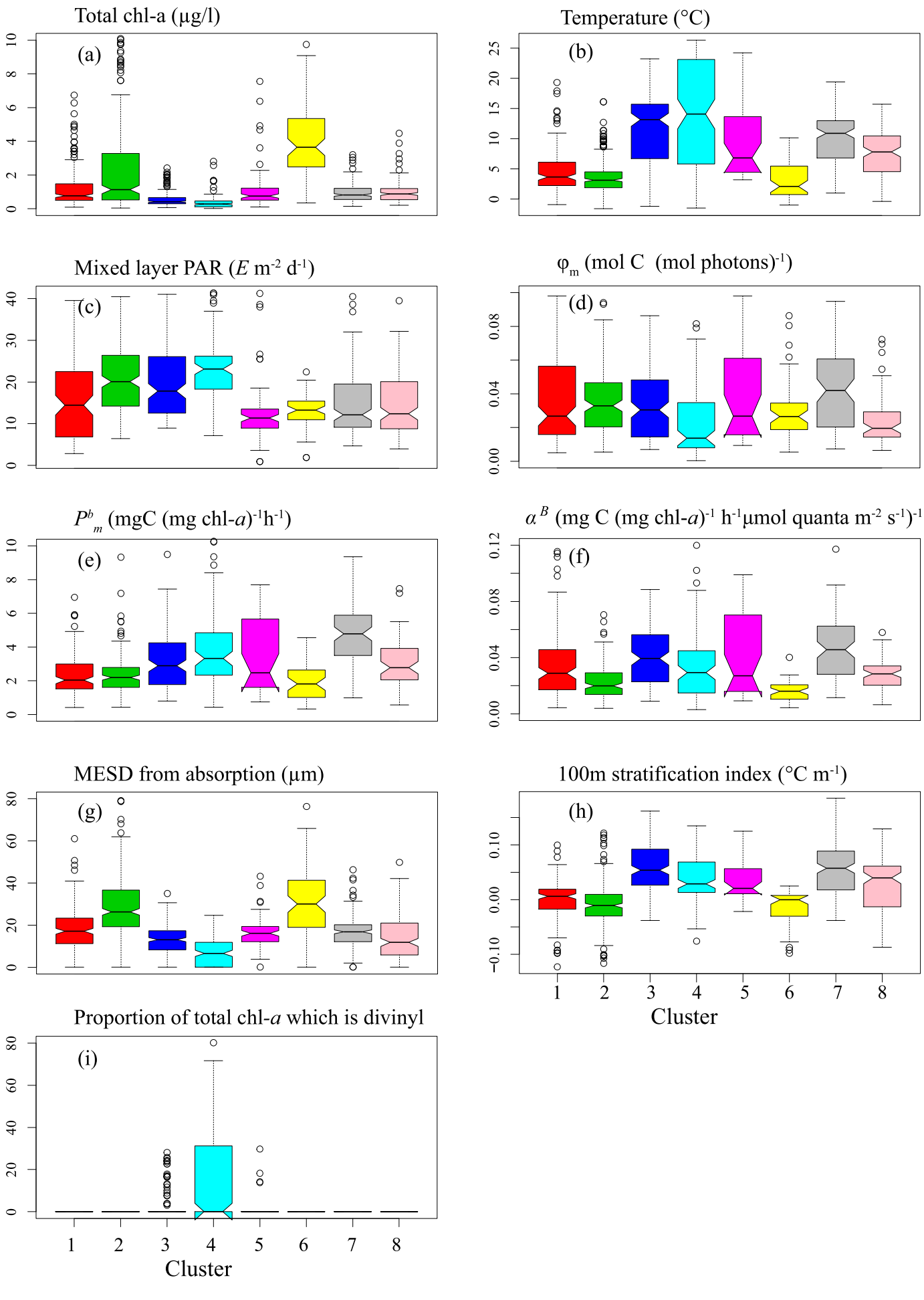
Total chl-a (µg/l)
(a)
0
2
4
6
8
10
Temperature (°C)
(b)
0
5
10
15
20
25
Mixed layer PAR (E m-2 d-1)
(c)
0
10
20
30
40
φm (mol C (mol photons)-1)
(d)
0.00
0.04
0.08
Pbm (mgC (mg chl-a)-1h-1)
(e)
0
2
4
6
8
10
α B (mg C (mg chl-a)-1 h-1µmol quanta m-2 s-1)-1
(f)
0.00
0.04
0.08
0.12
MESD from absorption (µm)
(g)
0
20
40
60
80
100m stratification index (°C m-1)
(h)
−0.10
0.00
0.10
1
2
3
4
5
6
7
8
Cluster
Proportion of total chl-a which is divinyl
(i)
0
20
40
60
80
1
2
3
4
5
6
7
8
Cluster

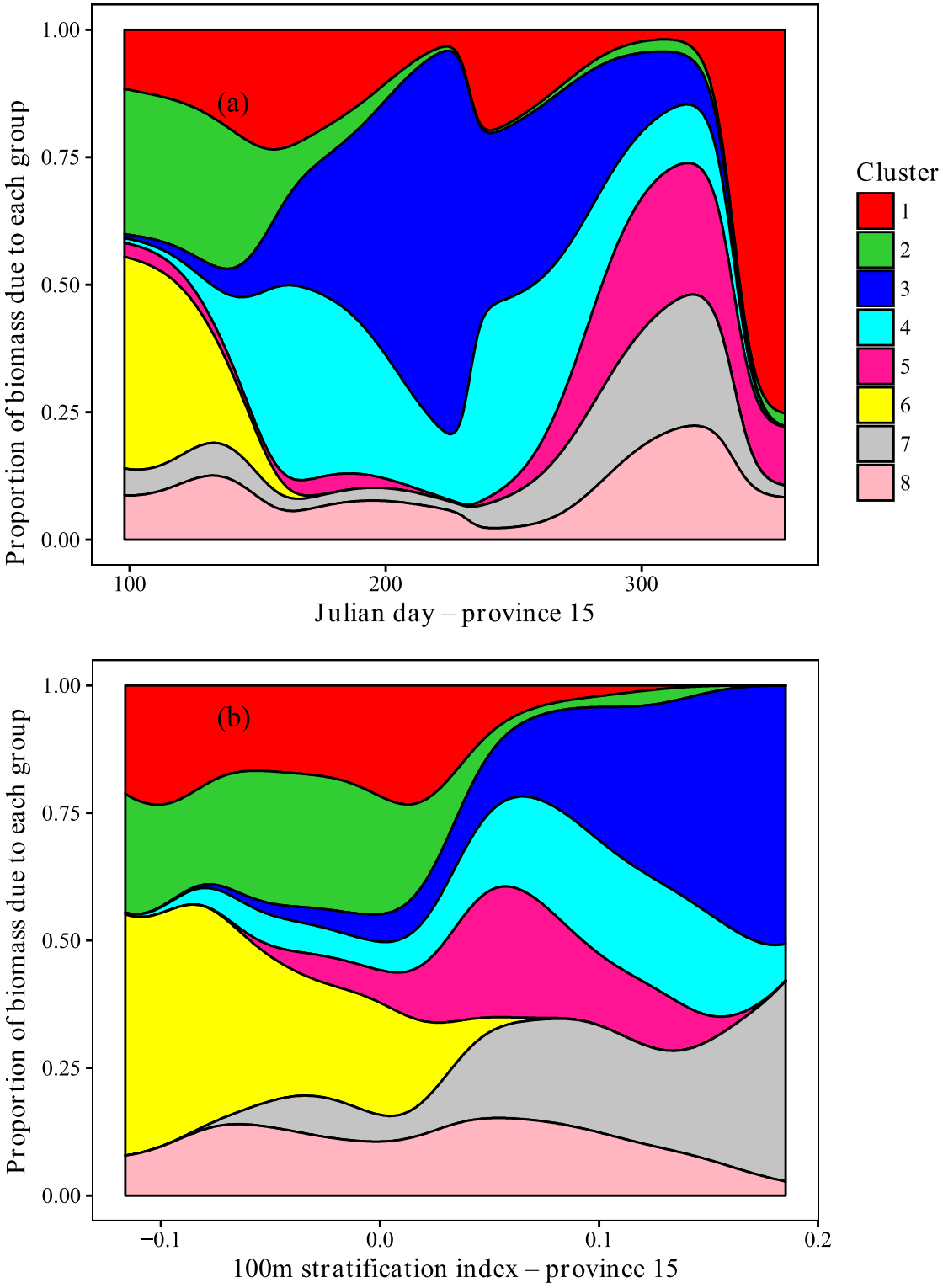
(a)
1.00
0.75
0.50
0.25
0.00
Proportion of biomass due to each group
100
200
300
Julian day – province 15
Cluster
1
2
3
4
5
6
7
8
(b)
1.00
0.75
0.50
0.25
0.00
Proportion of biomass due to each group
−0.1
0.0
0.1
0.2
100m stratification index – province 15

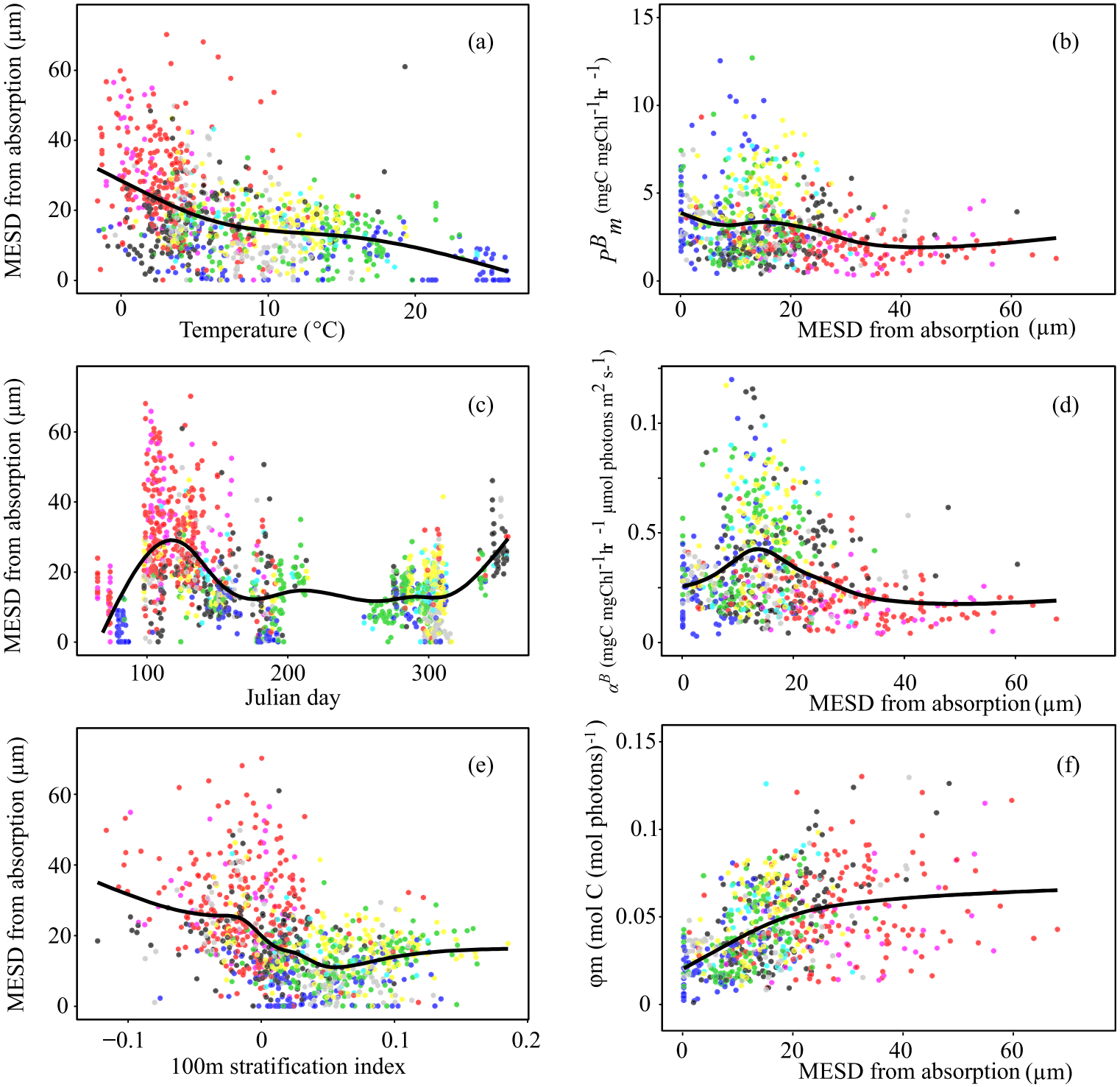
(a)
MESD from absorption (µm)
Temperature (°C)
(b)
P^B_m (mgC mgChl^{-1}hr^{-1})
MESD from absorption (µm)
(c)
MESD from absorption (µm)
Julian day
(d)
α^B (mgC mgChl^{-1}hr^{-1} µmol photons m^2 s^{-1})
MESD from absorption (µm)
(e)
MESD from absorption (µm)
100m stratification index
(f)
φm (mol C (mol photons)$^{-1}$)
MESD from absorption (µm)

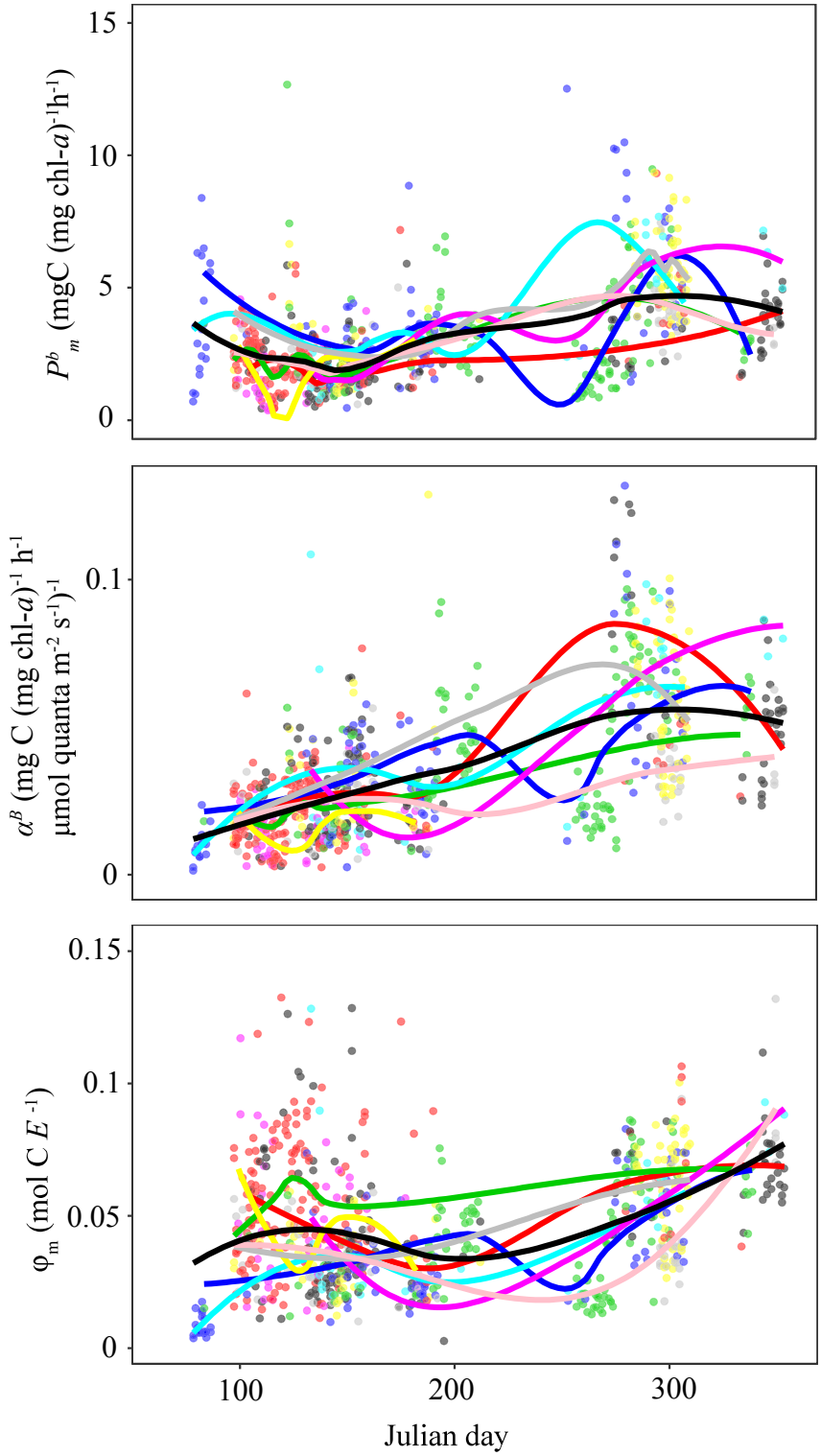
15
10
5
0
P^b_m (mgC (mg chl-a)$^{-1}$h^{-1})
0.1
0
α^B (mg C (mg chl-a)$^{-1}$ h^{-1} µmol quanta m^{-2} s^{-1})$^{-1}$
0.15
0.1
0.05
0
φ_m (mol C E^{-1})
100
200
300
Julian day

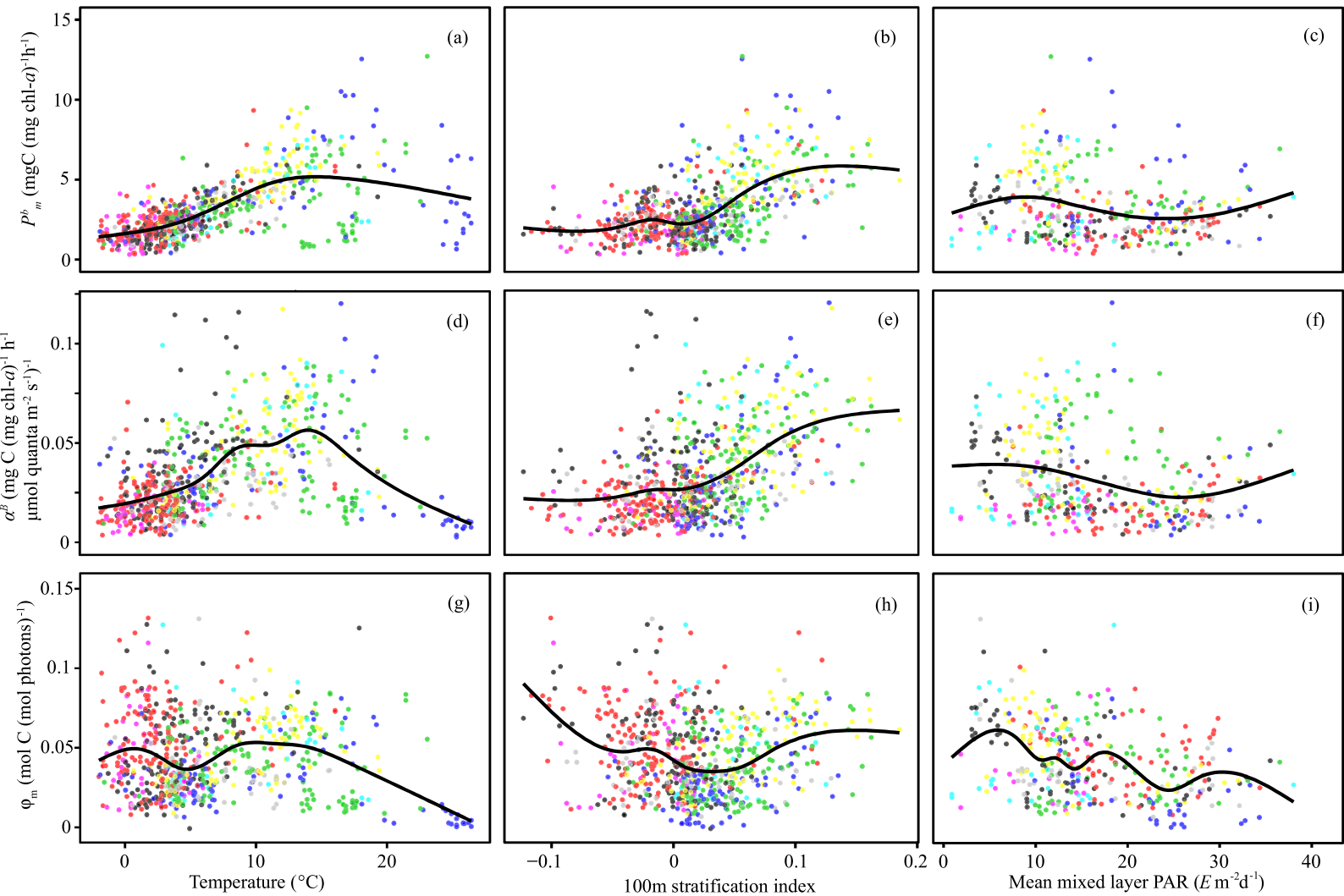
(a)
(b)
(c)
(d)
(e)
(f)
(g)
(h)
(i)
P^b_m (mgC (mg chl-a)$^{-1}$h^{-1})
α^B (mg C (mg chl-a)$^{-1}$ h^{-1} µmol quanta m^{-2} s^{-1})$^{-1}$
φ_m (mol C (mol photons)$^{-1}$)
Temperature (°C)
100m stratification index
Mean mixed layer PAR (E m^{-2}d^{-1})